JCB Journal of Cell Biology

ARTICLE

Ca^{2+} transients in melanocyte dendrites and dendritic spine-like structures evoked by cell-to-cell signaling

Rachel L. Belote and Sanford M. Simon

Melanocytes are the neural crest–derived pigment-producing cells of the skin that possess dendrites. Yet little is known about how melanocyte dendrites receive and process information from neighboring cells. Here, using a co-culture system to interrogate the interaction between melanocyte dendrites and keratinocytes, we show that signals from neighboring keratinocytes trigger local compartmentalized Ca^{2+} transients within the melanocyte dendrites. The localized dendritic Ca^{2+} transients could be triggered by two keratinocyte-secreted factors, endothelin and acetylcholine, which acted via specific melanocyte receptors. Furthermore, compartmentalized Ca^{2+} transients were also generated on discrete dendritic spine-like structures on the melanocytes. These spines were also present in intact human skin. Our findings provide insights into how melanocyte dendrites communicate with neighboring cells and offer a new model system for studying compartmentalized signaling in dendritic structures.

Introduction

As the pigment-producing cells of the skin, melanocytes have melanosomes, specialized lysosome-related organelles. Melanin pigment is made within the lumen of melanosomes and transferred, via melanocyte dendrites, to neighboring keratinocytes, epithelial cells that comprise the bulk of the epidermis (Marks and Seabra, 2001; Wu and Hammer, 2014). Keratinocytes are known regulators of melanocyte behavior, and much work has been done to understand how keratinocytes influence melanocyte cell proliferation and the production and transfer of pigment throughout the skin (Gordon et al., 1989; Hirobe, 2014). Nonetheless, cell–cell communication between melanocytes and keratinocytes, at the single-cell level, is poorly understood.

Epidermal melanocytes reside within the basal layer of the epidermis in a ratio of ∼1:10 with basal keratinocytes (Adameyko et al., 2009; Erickson et al., 1992; Fitzpatrick and Szabo, 1959). This arrangement has led to the proposal that there are pigmentary units across the epidermis in which one melanocyte, through its dendrites, interacts with ∼30–40 neighboring keratinocytes (Fitzpatrick and Breathnach, 1963; Jimbow et al., 1976). However, it remains unclear how each melanocyte dendrite responds to input from adjacent keratinocytes. Studies of other cell types with branched morphologies have shown that long branched cell extensions are capable of localized cell–cell signal through spatial restriction in second messengers such at Ca^{2+} (Llinás and Hess, 1976; Llinás et al., 1968; Spencer and Kandel, 1961; Yuste and Denk, 1995). Here we explore how melanocytes use their dendrites to interact with and receive information from keratinocytes using a co-culture of melanocytes and keratinocytes and an ultra-structure level interrogation of intact human skin. We show that endothelin and acetylcholine (ACh) secreted by keratinocytes elicit local and compartmentalized Ca^{2+} transients in melanocyte dendrites. In addition, we characterize restricted Ca^{2+} transients in spine-like structures on melanocyte dendrites co-cultured with keratinocytes. The dendritic spines were also seen on melanocytes in intact human skin, where they were surrounded by keratinocytes, which contained vesicles in their cytoplasm adjacent to the melanocyte spines.

Results

Optimized co-culture for the study of melanocyte dendrite cell–cell interactions

In intact human skin, melanocyte dendrites extend throughout the layers of the epidermis (Fig. 1 A and Fig. S1). This allows each melanocyte, at both its cell body and dendrites, to interact with multiple neighboring keratinocytes. We sought to recapitulate this arrangement in an in vitro culture system that would allow us to resolve melanocyte–keratinocyte interactions at the dendritic level.

Building upon previous studies, we created a co-culture of melanocytes and keratinocytes containing both keratin 14

Laboratory of Cellular Biophysics, Rockefeller University, New York, NY.

Correspondence to Rachel L. Belote: rachellbelote@gmail.com; Sanford M. Simon: simon@rockefeller.edu.

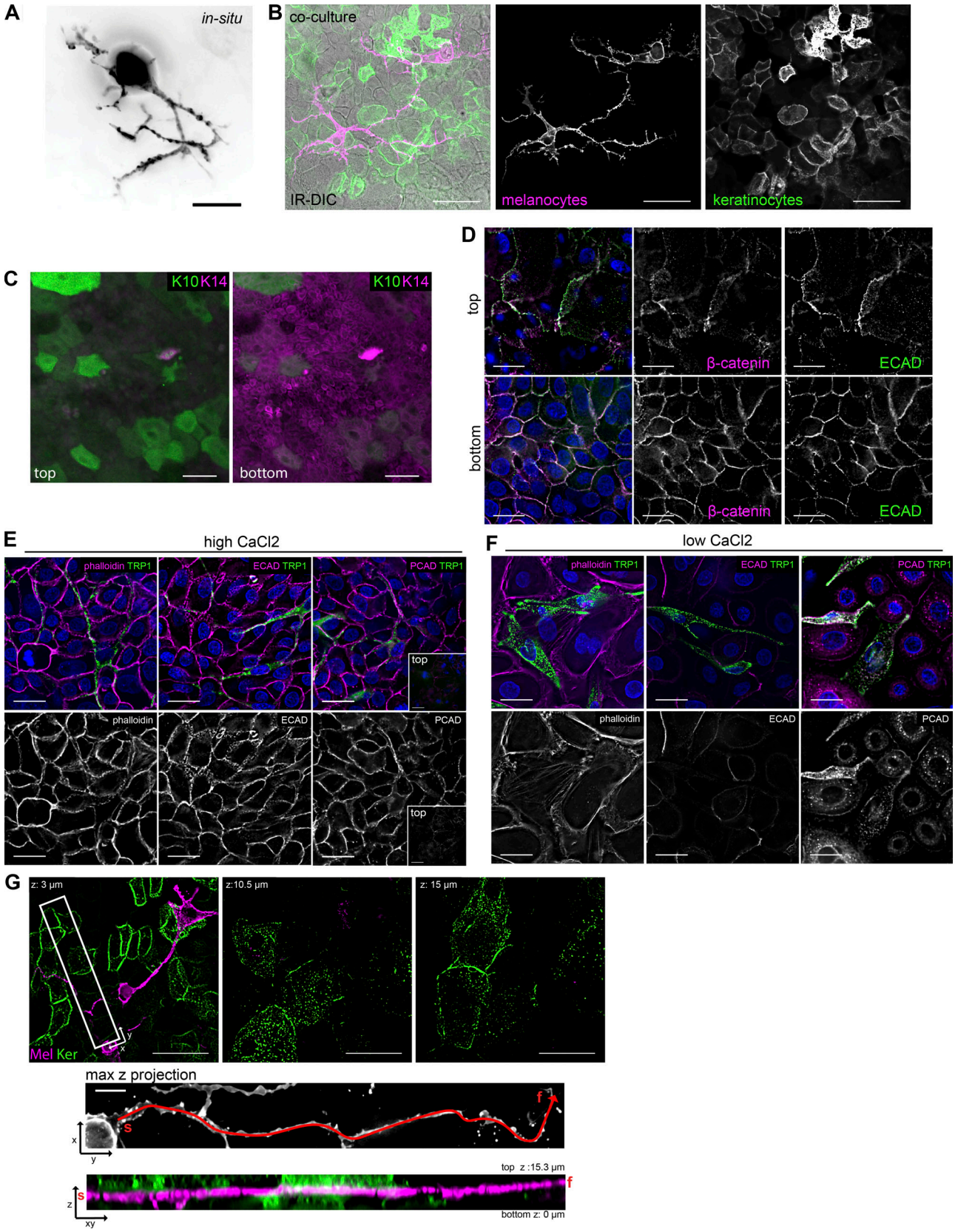

Figure 1. **Optimized melanocyte–keratinocyte co-culture for studying cell–cell interactions. (A)** Dendritic branching of an individual melanocyte within an intact epidermal sheet, microinjected with Lucifer yellow. **(B)** Melanocytes in co-cultures have similar morphology to melanocytes in situ (A). Mosaic labeled melanocytes (iRFPmem, magenta) and keratinocyte (eGFPmem, green) in the bottom layer of mature co-culture. **(C)** Both K14-positive keratinocytes (basal layer) and keratinocytes with varying levels of K10 (top layer) are present in co-cultures. **(D)** ECAD cell–cell adhesion is present in all layers of the co-culture

and colocalizes with β-catenin. **(E)** Cells in co-cultures with high (1.06 mM) $CaCl_2$ have morphologies (as assayed by F-actin using phalloidin) and cell–cell adhesion (as assayed by ECAD and PCAD) consistent with intact skin (Fig. S1). Phalloidin and ECAD: representative images from the bottom layer of co-culture. PCAD: representative image of bottom layer and top layer (inset). **(C–E)** Hoechst was used for nuclear stain. **(F)** Co-cultures maintained in low (0.06 mM) $CaCl_2$ do not have morphologies and cell–cell adhesion similar to intact skin (Fig. S1). **(G)** Co-cultured melanocyte dendrites (magenta, iRFPmem) interact with keratinocytes (green, EGFPmem) in the bottom and upper layers of the co-culture. Z, XY image from red line in maximum z projection. "s" corresponds to start of dendrite, and "f" corresponds to final point of the dendrite. Scale bars, (A) 15 µm; (B) 50 µm; (C) 25 µm; (D) 200 µm; (E) 25 µm; (F) 25 µm; and (G) 50 µm.

(K14)– and keratin 10 (K10)–positive keratinocytes (De Luca et al., 1988; Lei et al., 2002; Valyi-Nagy et al., 1993). Mature co-cultures were achieved by seeding at a high density (0.5×10^4 melanocytes and 5×10^4 keratinocytes per 78 mm^2), to achieve 100% confluence, and increasing the $CaCl_2$ concentration of the growth media from 0.06 mM $CaCl_2$ to 1.06 mM $CaCl_2$ for 2 d. This resulted in cultures that contained a bottom layer of cells comprised of melanocytes and K14-positive keratinocytes (Fig. 1, B and C). K10-positive keratinocytes were present above the bottom layer in one to two additional cell layers, which varied throughout the culture (Fig. 1 C). Mature co-cultures exhibited cell morphologies and cadherin-based cell–cell adhesion (Fig. 1, D and E) consistent with intact skin (Fig. S1, D and E; Tinkle et al., 2004), whereas co-cultures maintained in low (0.06 mM) $CaCl_2$ growth media did not (Fig. 1 F). E-cadherin (ECAD) and β-catenin colocalized in all layers of the mature co-cultures, while only the bottom layer of the co-cultures expressed high levels of P-cadherin (PCAD; Fig. 1, D and E). Importantly, melanocytes exhibited morphologies similar to those from intact epidermal sheets (Fig. 1, A and B; and Fig. S1 D) and made contact with numerous surrounding keratinocytes within and above the bottom layer of cells (Fig. 1 G).

To visualize melanocytes and keratinocytes in living cultures, the two cell types were cultured separately, and then a subset of each population was transduced with lentivirus encoding a fluorescent protein plasma membrane reporter: EGFPmem (melanocytes) or iRFPmem (keratinocytes). After 24 h, both cell types were combined to initiate the co-culture (Fig. 1 B). Mosaic labeling of each cell type allowed for real-time morphological observation of individual cells in the dense 3D culture. In regions with only a few labeled keratinocytes, we observed processes that extended from the cell surface of the keratinocytes, which contacted and wrapped adjacent melanocyte dendrites (Fig. 2 A). The keratinocyte processes and melanocyte dendrites made a stable interaction, which was maintained over the course of an hour even while each of the processes was moving (Fig. 2, B and C).

In intact human skin, similar interactions were observed from thin transmission EM (TEM) sections. Processes from basal and suprabasal keratinocytes enveloped melanocyte dendrites in multiple layers of overlapping projections (Fig. 2 D), often physically isolating multiple dendrites within the same region (Fig. 2 E). Interestingly, some keratinocytes had pools of small vesicles (44–70 nm diameter) in the cytosol adjacent to the plasma membrane that was juxtaposed to the melanocyte dendrite (Fig. 2 E, right panel). These pooled vesicles were distinct in their aggregated localization from other intracellular vesicles present throughout the cytosol of all cells and suggested that melanocyte dendrites might receive localized signaling from individual keratinocytes. To confirm that the keratinocyte processes observed in situ were indeed wrapping around melanocyte dendrites, focused ion beam scanning EM (FIB-SEM) was used to obtain serial sections of intact neonatal foreskin with a volume of 30 × 27 × 27 µm at 30 nm z resolution and an XY pixel size of 14–18 nm. 3D reconstruction of two keratinocyte processes showed that both processes interacted with and wrap around the melanocyte dendrite (Fig. 2, F–H).

Melanocyte dendrites have compartmentalized Ca^{2+} transients

Keratinocytes secrete multiple paracrine factors that influence melanocyte behavior (Gordon et al., 1989; Hirobe, 2014), some of which activate canonical cell–cell signaling cascades that use Ca^{2+} as a second messenger. Thus, we used the genetically encoded Ca^{2+} sensor GCaMP6f (Chen et al., 2013) to monitor cytosolic Ca^{2+} in the melanocytes. To ensure co-cultures were imaged in the absence of exogenous growth factors or serum, cells were washed three times with PBS and then imaged in a modified Dulbecco's PBS (DPBS) containing 1.06 mM $CaCl_2$ and no additional growth factors or serum (see Materials and methods). Unless stated otherwise, all subsequent Ca^{2+} imaging was conducted in the absence of exogenous growth factors or serum. Most melanocytes (64 ± 11%, mean ± SD, n = 22 co-culture cultures), co-cultured with keratinocytes in the absence of exogenous growth factors, had spontaneous Ca^{2+} transients over an observation period of 2.5 min (Fig. 3, A and B; and Video 1). The majority of Ca^{2+} transients were localized fluctuations in Ca^{2+} that occurred in the dendrites (Fig. 3, A–C; and Fig. 4), with few localized fluctuations within the cell body (Fig. 3, C and D) and few global transients throughout the whole cell (Fig. 3, A, C, and E).

Dendritic Ca^{2+} transients are keratinocyte-dependent

To determine if the dendritic transients of Ca^{2+} were intrinsic to melanocytes or were dependent on the presence of keratinocytes, we altered the growth conditions and cell types present in cultures of melanocytes expressing GCaMP6f. Cultures were then imaged in modified DPBS without serum or other exogenous growth factors. The high percentage of melanocytes with Ca^{2+} transients (64 ± 11%) was only observed when melanocytes were co-cultured with keratinocytes. Significantly, fewer melanocytes had Ca^{2+} transients when the keratinocytes were replaced with HEK293T cells (Fig. 3 F, 10 × 293T: 13 ± 6%) or melanocytes were grown in mono-culture (Fig. 3 F, 10 × Mel and Mel alone: 16 ± 2% and 11 ± 4%, respectively), or when melanocytes were separated from keratinocytes by a semiporous membrane (Fig. S2 B, TW 10 × Ker: 9 ± 8% to 20 ± 10%, depending on growth conditions). This was irrespective of growth media formulation (Fig. S2, A and B). In co-cultures, the number

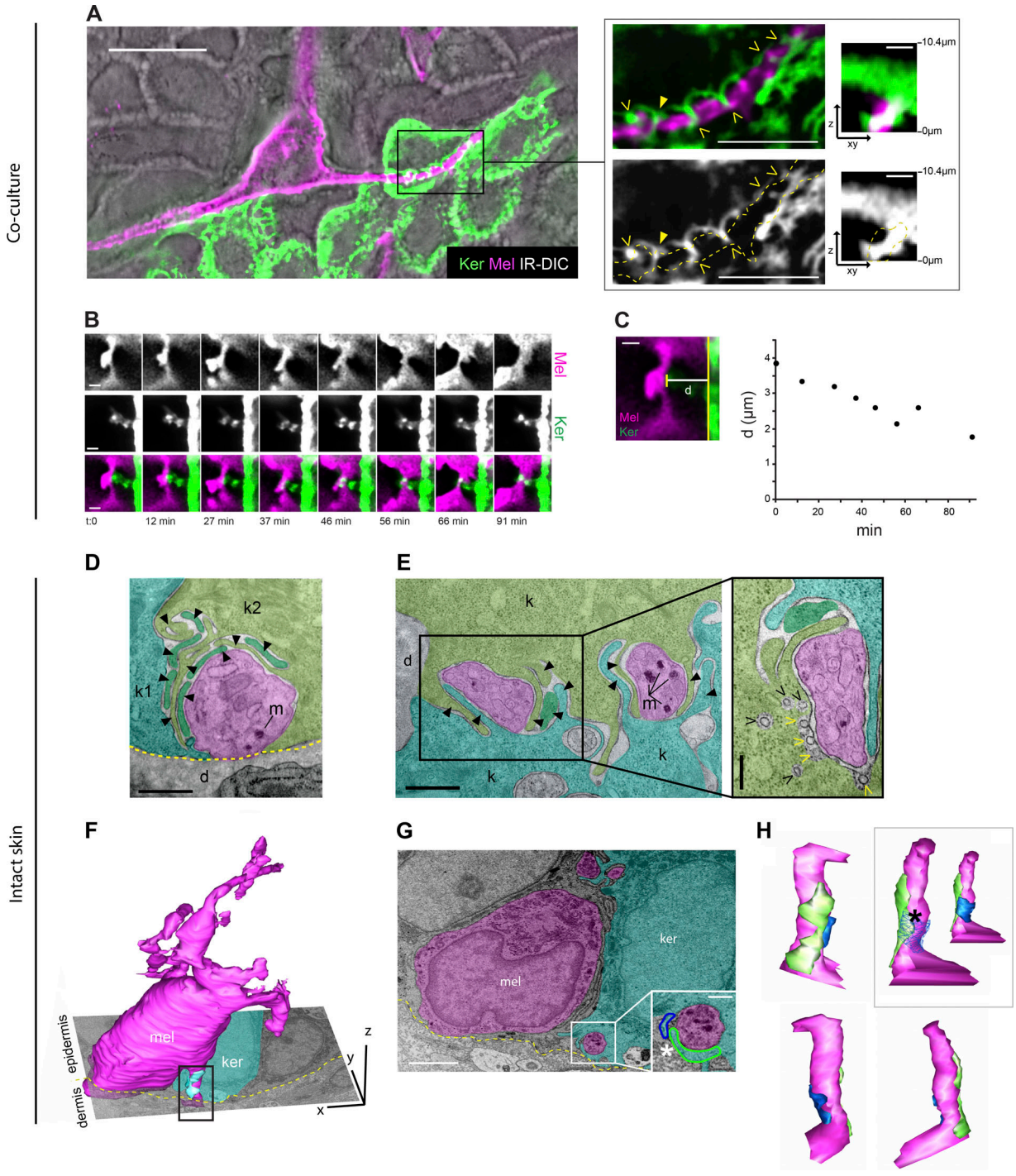

Figure 2. **Keratinocyte processes interact with melanocyte dendrites. (A)** Keratinocyte processes (yellow arrowheads) wrap around melanocyte dendrites in the optimized co-culture system. Representative image from bottom layer of co-culture. Z, XY images are from lines draw through the keratinocyte process marked by the closed arrowhead. **(B)** Keratinocyte process remains in contact with melanocyte dendrite during changes in morphology and location. Time lapse imaging of a keratinocyte projection interacting with a melanocyte dendrite. **(C)** Melanocyte dendrite displacement relative to the keratinocyte cell body during interaction with the keratinocyte process. Distance (d) was measured between the melanocyte dendrite (short yellow line) and the closest edge of the keratinocyte cell body (long yellow line). **(D–H)** Keratinocyte processes wrap around melanocyte dendrites in intact human skin. **(D)** TEM cross-section of intact neonatal foreskin. Melanocyte dendrites (magenta) are surrounded by keratinocyte (k1, teal; k2, green) processes (filled arrowheads); dashed yellow line, basement membrane; d, dermis; m, melanosome. **(E)** Left: Keratinocyte processes physically separate adjacent melanocyte dendrites. Right: Pool of small vesicles (arrowhead) within the keratinocyte (k) adjacent to melanocyte dendrite. Yellow arrowhead, vesicles fused with the keratinocyte plasma membrane. **(F)** 3D reconstruction of a melanocyte (magenta) and keratinocyte (cyan) processes (boxed region) from intact neonatal foreskin using 30-nm serial FIB-SEM. Yellow line demarcates epidermal–dermal junction. **(G)** Representative FIB-SEM image from the reconstruction in F. Inset: melanocyte dendrite surrounded by adjacent keratinocyte with two processes (blue, green). **(H)** Multiple angles from the 3D reconstruction in F with the two keratinocyte processes (blue, green) that overlap each other (marked by asterisk in box) from G. Scale bars, (A) 25 µm, inset, 10 µm, z-xy, 1.5 µm; (B) 2 µm; (C) 2 µm; (D) 0.6 µm; (E) left, 0.6 µm, inset, 0.25 µm; (G) 2 µm, inset, 0.5 µm.

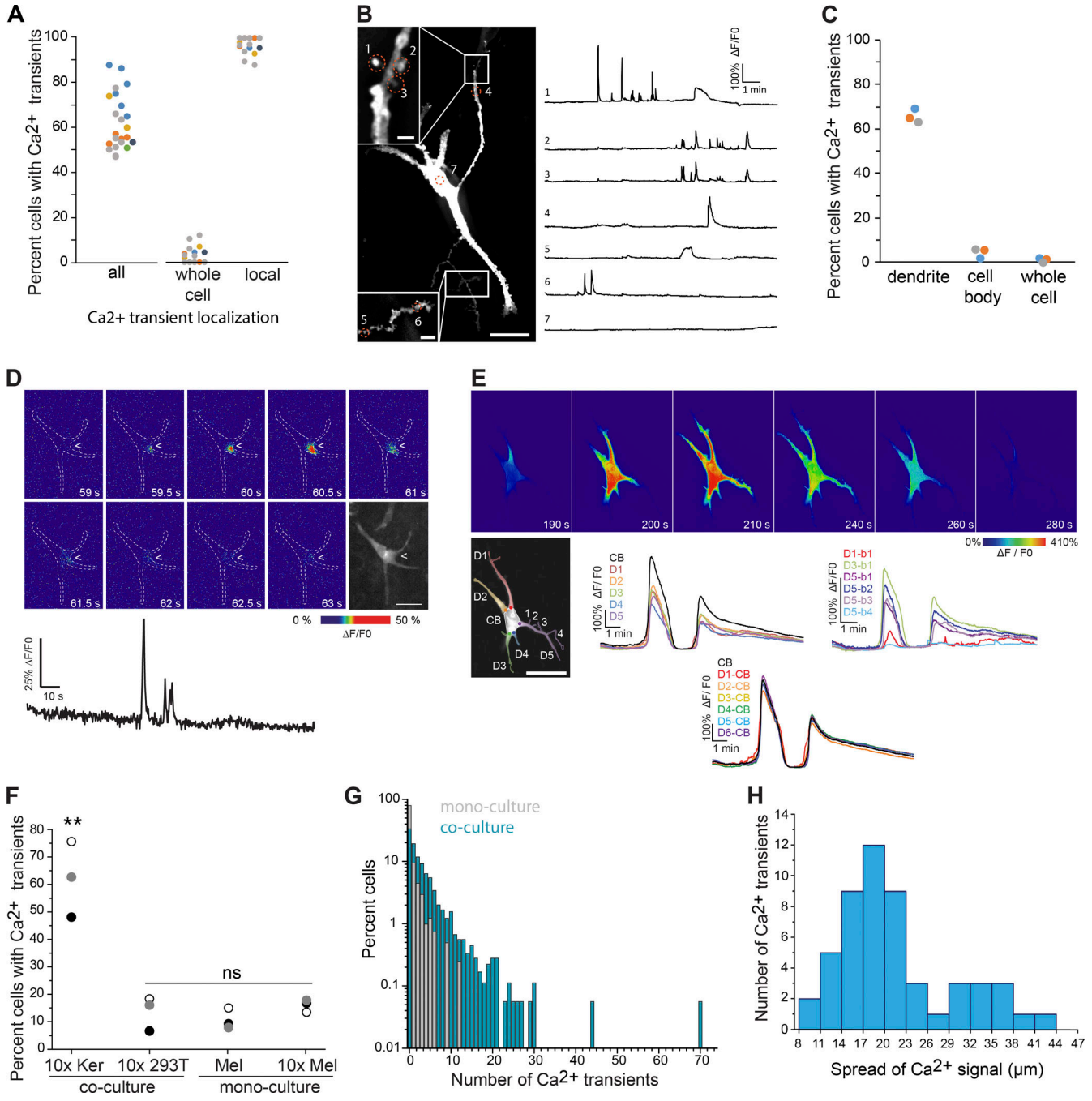

Figure 3. **Melanocytes co-cultured with keratinocyte have local fluctuations in cytosolic Ca^{2+} in the absence of exogenous growth factors. (A)** The majority of co-cultured melanocytes, in the absence of exogenous growth factors, have at least one Ca^{2+} transient when co-cultured with keratinocytes (n = 22 co-cultures; color indicates skin donor, n = 6). See also Video 1. Of the melanocytes with transients, the majority had local Ca^{2+} transients, while few had global whole cell Ca^{2+} transients. **(B)** Local Ca^{2+} transients occur at different regions and different times within GCaMP6f expressing melanocytes in co-culture with keratinocytes. **(C)** The majority of local Ca^{2+} transients are in melanocyte dendrites (n = 3 co-cultures from three different donors randomly chosen from A). **(D)** Representative cell body Ca^{2+} transient that is localized to a small region of the cell body with corresponding ΔF/F0 plot from ROI at the center of the of the transient. **(E)** Representative whole cell Ca^{2+} transient with corresponding ΔF/F0 plot from designated regions: CB, cell body; DX, primary dendrites where X indicates dendrite number; DX-CB, dendrite–cell body junction; DX-by, secondary dendrites; y indicates secondary branch number. **(F)** Melanocytes in co-cultures with 10× keratinocytes (10xKer, the normal ratio of keratinocyte to melanocytes in co-cultures) have significantly more Ca^{2+} transients than those co-cultured with HEK293Ts (10× 293T), alone (Mel, normal melanocyte seeding density but no added keratinocytes), or with 10× melanocytes (10xMel, GCaMP6f melanocytes culture with an additional 10× melanocytes not expressing GCaMP6f); n = 3 co-cultures per condition; colors indicate different skin donors. One-way ANOVA $F(3,8) = 29.05$, $P = 0.00012$; post hoc Tukey means comparison to other culture conditions, **, $P = 0.005$. See also Fig. S2. **(G)** Distribution of the number of transients per cell for co-cultured melanocytes (data from A and one additional donor; n = 1,793 melanocytes from 27 co-cultures from seven different skin donors) and mono-cultured melanocytes (inset, n = 563 melanocytes from five co-cultures of different skin donors). **(H)** Distribution of the spatial spread of the Ca^{2+} signal (full-width half maximum Gaussian fit) at peak ΔF/F0 intensity for transients within the dendrites of co-cultured melanocytes (n = 53 dendrites from 11 co-cultures from three different skin donors). For all Ca^{2+} imaging, growth media were removed, and cultures were washed three times then imaged in a modified DPBS solution with no growth factors or serum. Scale bars, (B) 25 μm, top, 2 μm, bottom, 5 μm; (D) 75 μm; (E) 100 μm.

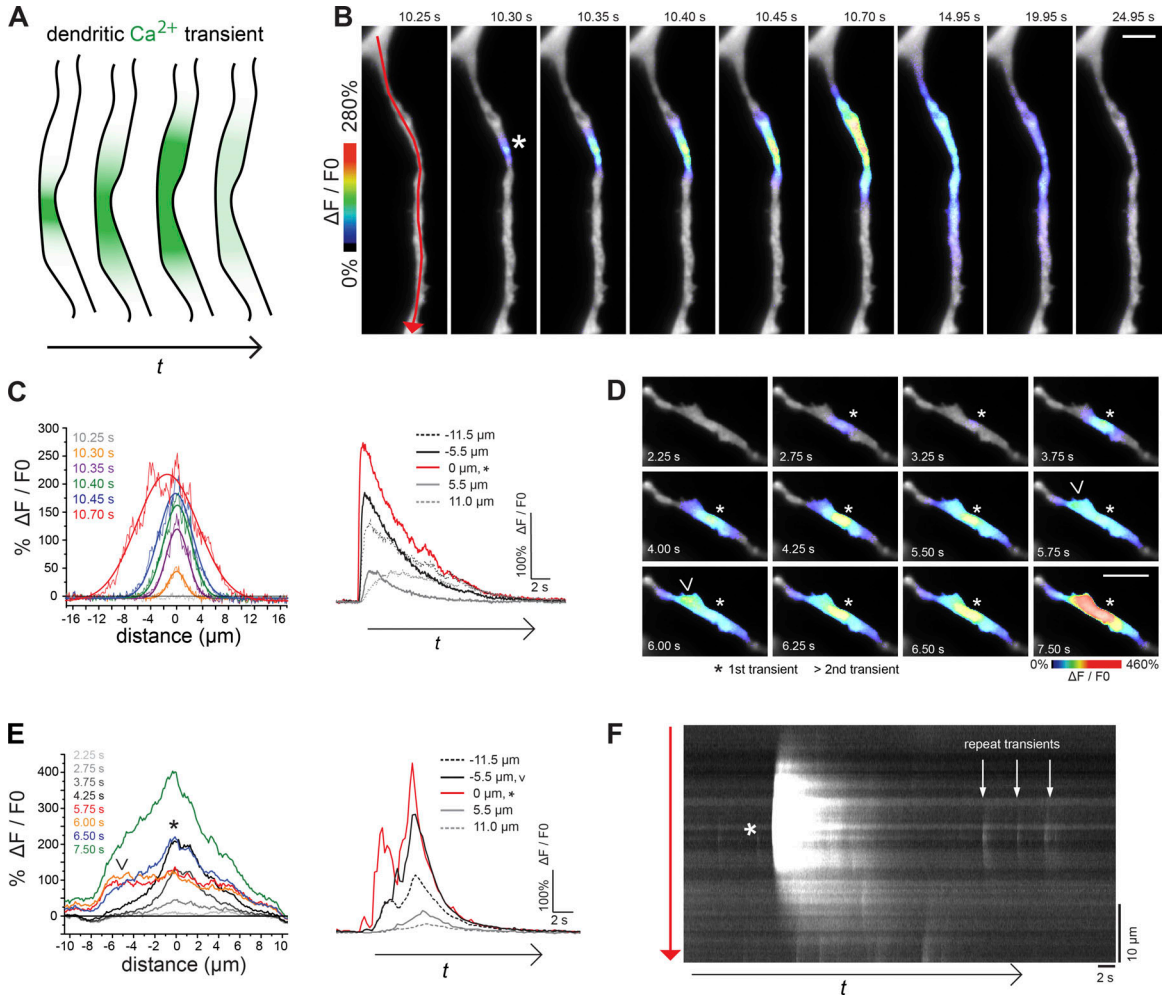

Figure 4. **Spatiotemporal characterization of localized dendritic Ca^{2+} transients. (A)** Schematic of dendritic Ca^{2+} transient (green) spread from one origin over time (t). **(B)** Dendritic Ca^{2+} transient from single detectable origin site (*). **(C)** Ca^{2+} spread at six time points (full-width half maximum Gaussian fit as thick lines) and time courses at five distances from the initiation sight (*) in the single dendrite (B). **(D)** Time-lapse imaging of Ca^{2+} transients originating at two adjacent regions (* and >) in a single co-cultured melanocyte dendrite. **(E)** Spatiotemporal dynamics of a single representative dendritic transient. Left: Ca^{2+} spread at the eight corresponding times marked in D. Right: Time course of Ca^{2+} transients at the five indicated distances from the initiation site (*); region > is represented at −5.5 µm with solid black line. **(F)** Kymograph of line along the dendrite in B. Repetitive Ca^{2+} transients (white arrows) following the transient (*) in B. Scale bars, (B) 5 µm; (D) 5 µm. See also Video 2.

of local dendritic transients detected during 2.5 min ranged from 0–70 per melanocyte. Of the melanocytes with local dendritic transients, 91% had 1–9 transients while 9% had >10 transients (Fig. 3 G). In comparison, of the few mono-cultured melanocytes that had dendritic transients, 90% had 1–4 transients and 10% had 5–12 transients (Fig. 3 G, inset). Thus, close proximity to, and possibly direct contact with, keratinocytes was required for the high frequency of Ca^{2+} transients.

Analysis of dendritic Ca^{2+} transients from 53 melanocytes grown with keratinocytes in co-culture media showed a range of detectable Ca^{2+} spread from 8–42 µm with the majority (58%) of transients being 14–22 µm in length (Fig. 3 H). Individual dendrites had transients that either originated from a single point (Fig. 4, A–C; and Video 2) or from multiple distinct locations within a region several microns long of the dendrite (Fig. 4, D and E). In those dendrites that had multiple Ca^{2+} transients over time, repetitive transients initiated from the same region of the dendrite (Fig. 4 F).

To determine the source of Ca^{2+} responsible for the dendritic transients, we quantified the number of Ca^{2+} transients before and after the removal of external $CaCl_2$ and/or addition of 1 µM thapsigargin, which releases Ca^{2+} from internal stores (Lytton et al., 1991). The percentage of melanocytes with Ca^{2+} transients was reduced by either removal of external $CaCl_2$ or addition of thapsigargin to the imaging media (0.63 ± 0.04 and 0.30 ± 0.05 fold change from before treatment, respectively) compared with the control (0.88 ± 0.5 fold change from before treatment), with the combination of removal of $CaCl_2$ and addition of thapsigargin having the greatest effect (0.07 ± 0.4 fold change from before treatment; Fig. 5 A). This was also true for the number of Ca^{2+} transients per cell (Fig. 5, B–E), where removal of external $CaCl_2$ plus the addition of thapsigarin reduced the number of

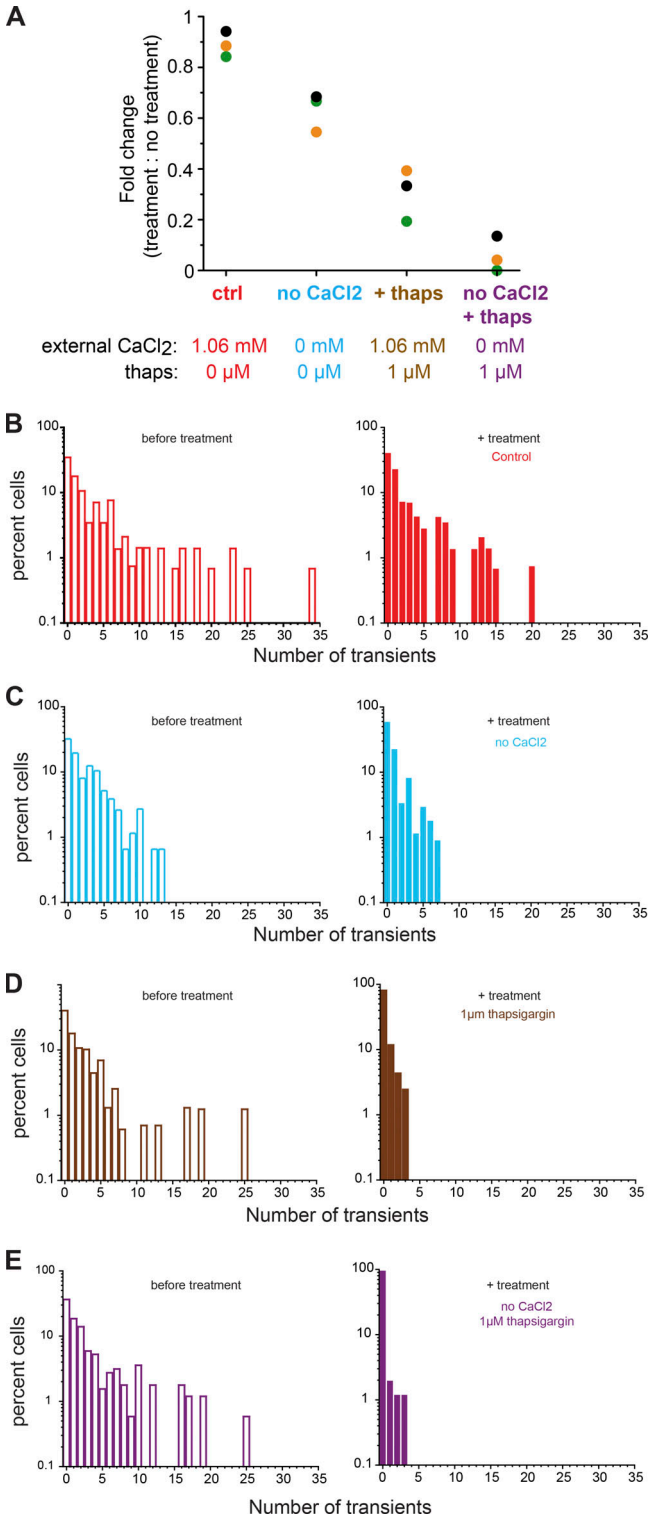

Figure 5. **External and internal Ca^{2+} pools contribute to melanocyte dendritic Ca^{2+} transients. (A)** Both removal of external$_2$ (no $CaCl_2$) and depletion of internal Ca^{2+} stores (+thaps) significantly reduce the number of dendritic Ca^{2+} transients in co-cultured melanocytes. *n* = 3 cultures per condition. Colors represent different skin donor. Significant by one-way ANOVA with post hoc Tukey means comparison ($F[3,8] = 67.8$, $P < 0.00001$, Tukey: all P-values < 0.01). **(B–E)** Distribution of the number of dendritic Ca^{2+} transients from co-cultures in A. **(B)** Before and after control treatment. **(C)** Before and after external $CaCl_2$ removal. **(D)** Before and after addition of 1 µM thapsigargin. **(E)** Before and after external $CaCl_2$ removal and addition of 1 µM thapsigargin. Colors in B–E correspond to conditions labeled in A.

transients per cell to a level similar to that of mono-cultured melanocytes (Fig. S3 H and Fig. S4 D).

Keratinocyte derived paracrine factors contribute to dendritic Ca^{2+} transients

Endothelins, a family of 21 amino acid peptides, play a critical role in melanocyte development, maturation, and homeostasis within the epidermis (Reid et al., 1996). Epidermal keratinocytes produce and secrete endothelin 1 (ET-1; Yohn et al., 1993), which can elicit increases of Ca^{2+} in the cell bodies of melanocytes (Kang et al., 1998). Addition of 10nM ET-1 to co-cultures produced recurring Ca^{2+} transients across the entire melanocyte, including dendrites and the cell body (Fig. 6, A–D; Fig. S3 A; and Video 3). The percentage of melanocytes with a response to ET-1 was dose-dependent (Fig. S3 B), and the number of transients per melanocyte also increased with the addition of 10 nM ET-1 (Fig. 6 B). ET-1–induced increase of Ca^{2+} in melanocytes co-cultured with keratinocytes was blocked by preincubation with a selective inhibitor of endothelin receptor B (ET_B), BQ788, but not an inhibitor of endothelin receptor A (ET_A), BQ123 (Fig. 6 B; Fig. S2, C and D; and Video 4), consistent with previous work that showed many patient-derived human melanocytes do not express ET_A (Eberle et al., 1999). This was also true of melanocytes in mono-culture (Fig. S3, E–H).

The localized Ca^{2+} transients in melanocytes elicited by ET-1 (Fig. 6, C–E; and Video 3) resembled the spontaneous Ca^{2+} transients in co-cultures of melanocytes and keratinocytes without the addition of exogenous ET-1 (Fig. 4 and Video 1). To test if the spontaneous local Ca^{2+} transients in melanocytes was caused by keratinocyte secreted endothelin, we treated co-cultures with endothelin receptor antagonists. Co-cultures treated with the ET_B antagonist BQ788 had a significant reduction in the percentage of melanocytes with Ca^{2+} transients, but no change was observed in Ca^{2+} transients in co-cultures treated with the ET_A antagonist BQ123 (Fig. 7 A). To confirm that the effects were due to inhibition of the ET_B on melanocytes and not the inhibition of ET_B on keratinocytes, we used Dicer-substrate siRNA (DsiRNA) against EDNRA (the gene that encodes ET_A) or EDNRB (the gene that encodes ET_B) to reduce expression of either ET_A or ET_B in melanocytes before co-culture with keratinocytes. Consistent with the endothelin receptor antagonist data, knockdown of ET_B but not ET_A reduced the number of co-cultured melanocytes with Ca^{2+} transients (Fig. 7 B). We next knocked down EDN1, the ET-1 gene, in keratinocytes and found that co-cultures with keratinocytes expressing shRNA against EDN1 had significantly fewer melanocytes with Ca^{2+} transients (Fig. 7, C and D). Together, these data confirmed that keratinocyte-secreted endothelin acts on melanocyte ET_B to produce local dendritic Ca^{2+} transients.

The Ca^{2+} transients were reduced by using antagonists in the bath to inhibit ET_B, shRNA in the melanocytes to reduce expression of the EDNRB, or shRNA in keratinocytes to reduce

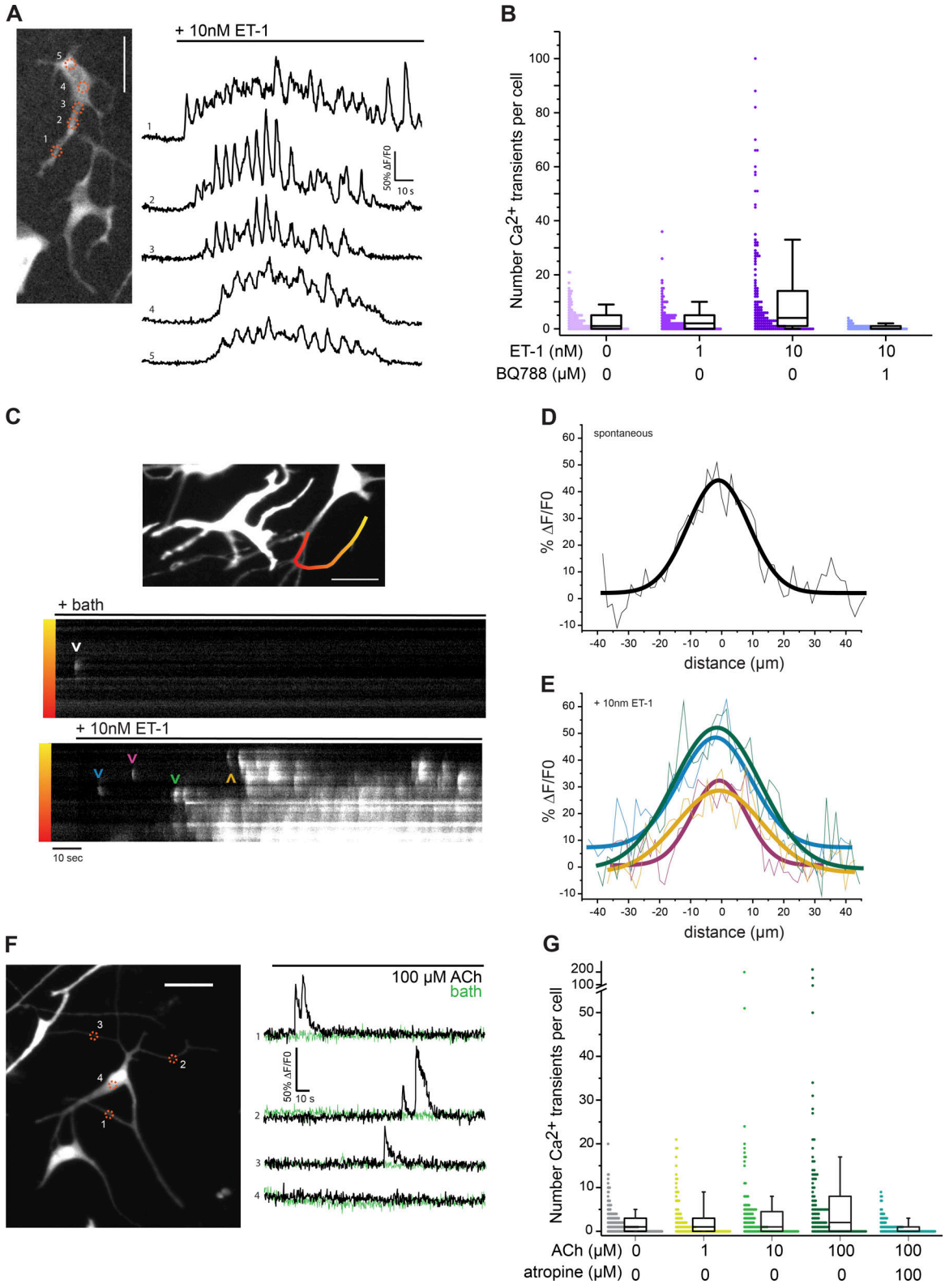

Figure 6. **Keratinocyte paracrine secreted factors ET-1 and ACh induce dendritic Ca^{2+} transients. (A)** Ca^{2+} oscillations in melanocytes co-cultured with keratinocytes in response to 10 nM ET-1 (black line: addition of 10nM ET-1 to imaging bath); ΔF/F0 plots corresponding to numbered regions on the melanocyte. See also Video 3. **(B)** ET-1 increases the number of Ca^{2+} transients per co-cultured melanocyte via the ET_B receptor (n = 203, 141, 141, and 62 cells from 3, 2, 2, and 1 different patient-derived and matched co-cultures, respectively). Significant by Kruskal-Wallis ANOVA (H = 67.63, 3 degrees of freedom [d.f.], P = 1.37 × 10^{-14}). Box: 25%, 75%; whiskers: 10–90%. **(C)** Co-cultured melanocyte dendritic Ca^{2+} transients induced by 10 nM ET-1. Top: Co-cultured melanocytes, expressing mCherry (shown) and GCaMP6f, before the addition of ET-1. Bottom: Kymograph (GCaMP6f) from corresponding color-coded line in top panel; black line denotes imaging media (left, "bath") or change to imaging media containing 10 nM ET-1 (right, +10 nM ET-1). **(D)** Ca^{2+} spread from a single

spontaneous dendritic transient before addition of ET-1, from > in kymograph in C. Thick line, full-width half maximum Gaussian fit. **(E)** Ca^{2+} spread from four dendritic transients after the addition of 10nM ET-1. Colors correspond to arrowheads with the same colors in the +10 nM ET-1 kymograph in C. Thick line, full-width half maximum Gaussian fit. **(F)** 100 µM ACh elicits local transient Ca^{2+} response in melanocyte dendrites. Black line: addition of ACh (black ΔF/F0 plot) or imaging media (bath, green ΔF/F0 plot). See also Video 5. **(G)** ACh, via mAChRs, increases the number Ca^{2+} transients per co-cultured melanocyte (n = 243, 128, 128, 115, and 131 cells from 4, 2, 2, 2, and 2 different patient-derived and matched co-cultures, respectively). Significant by Kruskal-Wallis ANOVA (H = 41.32, 4 d.f., P = 2.371×10^{-8}). Box: 25%, 75%; whiskers: 10–90%. Scale bars, 100 µm.

production of ET-1. However, none of these treatments eliminated the Ca^{2+} transients completely. In addition to production and release of endothelin, keratinocytes also possess the necessary cholinergic machinery to synthesize, release, and degrade the neurotransmitter ACh (Grando et al., 1993). It is also known that melanocytes express muscarinic receptors (mAChR) and respond to the mAChR specific agonist, muscarine (Buchli et al., 2001). Addition of ACh increased the number of Ca^{2+} transients per cell in co-culture (Fig. 6, F and G; Fig. S4 A; and Video 5) and mono-culture (Fig. S4, C and D), with some melanocytes having over 100 transients in 2.5 min, a 10-fold increase compared with control conditions (Fig. 6 G). Interestingly, ACh increased the frequency of Ca^{2+} transients in those cells that already showed activity, but had no effect on the number of melanocytes with Ca^{2+} transients (up to 100 µM; Fig. S4, A and B). This increase in frequency of Ca^{2+} transients, in both co- and mono-cultured melanocytes, was blocked by atropine, a selective muscarinic ACh receptor antagonist (Fig. 6 G and Fig. S4 D). To test if the spontaneous local Ca^{2+} transients in melanocytes resulted from release of ACh by keratinocytes, we treated co-cultures with muscarinic antagonist. Atropine decreased the number of co-cultured melanocytes with transients to 0.54 ± 0.08-fold compared with the results before treatment (Fig.7 E), indicating that endogenous ACh release contributed to melanocyte Ca^{2+}

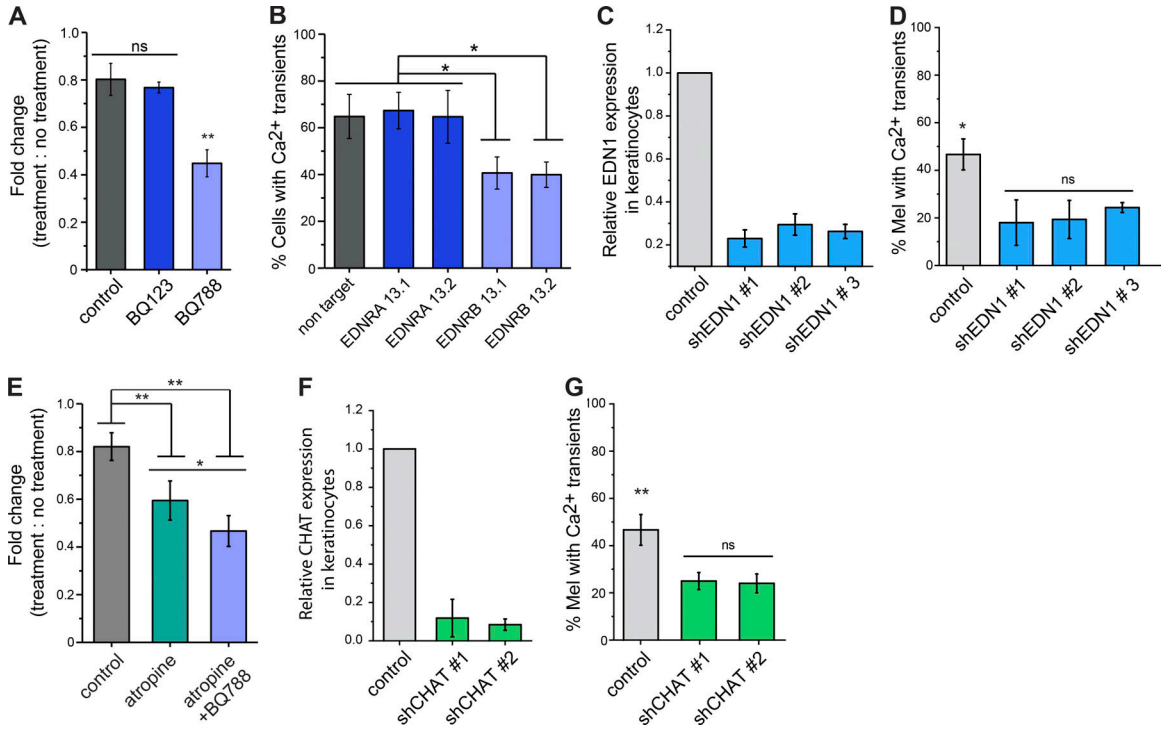

Figure 7. **Inhibition of endogenous endothelin and ACh signaling reduce melanocyte Ca^{2+} transients. (A)** Antagonism of ET_B (BQ788) but not ET_A (BQ123) significantly reduces the number of melanocytes with Ca^{2+} transients. Control: vehicle. n = 6, 3, and 3 co-cultures, respectively derived from six different donors. See also Video 4. One-way ANOVA F(2,9) = 39.38, P = 0.000035; post hoc Tukey means comparison to other culture conditions: **, P = 0.05; data represented as mean ± SD. **(B)** Knockdown of melanocyte ET_B (EDNRB 13.1 and 13.2) reduced the number of melanocytes with Ca^{2+} transients in co-cultures. One-way ANOVA F(4,10) = 8.21, P = 0.0033; post hoc Tukey means comparison to other culture conditions, *, P < 0.05; data represented as mean ± SD. n = 3 co-cultures. **(C)** Relative expression level of EDN1, determined by qRT-PCR, in keratinocytes transduced with three different shRNA against EDN1 normalized to GFP control. n = 3 technical replicates. **(D)** EDN1 knockdown in keratinocytes reduces the number of co-cultured melanocytes, expressing RCaMP1h, with Ca^{2+} transients. n = 3 co-cultures for each condition. One-way ANOVA F(3,8) = 10.5, P = 0.0037; post hoc Tukey means comparison to other culture conditions, *, P < 0.05. **(E)** mAChR antagonist atropine reduces the number of co-cultured melanocytes with Ca^{2+} transients. Control: vehicle. n = 5, 3, and 3 co-cultures, respectively, derived from five different donors. One-way ANOVA F(2,8) = 28.75, P = 0.00022; post hoc Tukey means comparison, **, P < 0.005; *, P = 0.10. **(F)** Relative expression level of CHAT, determined by qRT-PCR, in keratinocytes transduced with two different shRNA against CHAT, normalized to GFP control. n = 3 technical replicates. **(G)** CHAT knockdown in keratinocytes reduced the number of co-cultured melanocytes, expressing RCaMP1h, with Ca^{2+} transients. n = 3 co-cultures for each condition. One-way ANOVA F(2,6) = 20.7, P = 0.0020; post hoc Tukey means comparison to other culture conditions, **, P < 0.005. All data represented as mean ± SD.

transients. Addition of BQ788 with atropine reduced the number of melanocytes with transients by 0.47 ± 0.06-fold compared with the results before treatment (Fig.7 E), which was similar to the level of reduction observed when BQ788 alone was added. When we used shRNA to reduce expression of choline acetyltransferase (CHAT), the enzyme that synthesizes ACh from acetyl CoA and choline, in keratinocytes (Fig. 7 F), the number of melanocytes with Ca^{2+} transients was significantly less than that of the control. This confirmed that keratinocyte-secreted ACh contributes to local Ca^{2+} transients in melanocytes (Fig. 7 G).

Melanocytes have dendritic spine-like structures that can compartmentalize Ca^{2+}

Within co-cultures mosaically labeled with plasma membrane–localized fluorescent protein, we observed discrete spine-like structures protruding from melanocyte dendrites (Fig. 8 A), which was consistent with the small dendritic protrusions we observed on melanocytes injected with Lucifer yellow in epidermal sheets (Fig. S5 A). Spine-like structures present on the dendrites of the co-cultured melanocytes had variable morphologies: mushroom, stubby, thin, and cup-shaped (Fig. 8). These morphologies were distinct and different than the previously described melanocyte filopodia (Scott et al., 2002; Singh et al., 2010), which were also present on melanocyte dendrites (Fig. 8 A). The width of the spine heads ranged from 0.47 to 1.36 µm, and total lengths (from dendrite to tip of spine) were 0.55–2.75 µm (Fig. 8 C). The density of dendritic spine-like structures varied from dendrite to dendrite (1.6 ± 1.3 mean ± SD, spines per 10 µm) with some dendrites having no detectable spine-like structures (Fig. 8, D and E). The dendritic spine-like structures were surrounded by adjacent keratinocyte plasma membrane and contacted keratinocyte processes (Fig. 8, F and G). The morphology of some spines were stable (Fig. 8 G), while others were dynamic, moving 0.33–1 µm over an hour (Fig. 8 H).

In some cases, Ca^{2+} transients originated within and remained confined to resolvable spine-like structures (Fig. 9, A–D, panel 1; and Videos 6 and 7). Additionally, we observed Ca^{2+} transients near the perimeter of a dendrite and contained within a <2-µm region (Fig. 9, A–D, panels 2 and 3). These may be increases in Ca^{2+} within a spine-like structure protruding off the dendrite that could not be distinguishable in XY by fluorescence.

To test for the presence of dendritic spines on melanocyte dendrites in intact human skin at the ultrastructural level, we used TEM. In TEM images, melanocytes and their dendrites were distinguished from other cells by having a lighter, more electron-lucent cytoplasm, the presence of melanosomes within the cell body and dendrites, and a lack of desmosomes and lack of strong keratin filament staining. Melanosomes were also observed in keratinocytes, but keratinocytes were easily distinguished from melanocytes by the other criteria mentioned above. Using manual serial sectioning followed by TEM, we found examples of spine-like structures, which were indistinguishable from those observed in the melanocyte–keratinocyte co-cultures (Fig. 10 A and Fig. S4 A).

Due to the sparse density of melanocyte dendrites compared with the total cell mass of the epidermis, we used FIB-SEM to analyze more dendrites and visualize larger lengths of dendrites. We reconstructed four individual melanocytes among 16 surrounding keratinocytes within a volume of 30 × 27 × 27 µm at 30-nm z resolution and an XY pixel size of 14–18 nm. An example of one such melanocyte is shown in Fig. 2 F. Melanocytes were distinguished from other cell types by their dendritic morphology and lighter, more electron-lucent cytoplasm (Fig. S5 B). Individual melanocytes contacted 7 to 10 keratinocytes within the imaged volume, consistent with previous data (Fitzpatrick and Breathnach, 1963; Jimbow et al., 1976). All four melanocytes had spine-like structures (Table S1) with head widths of 0.14–0.72 µm and total lengths of 0.24–1.53 µm (Fig. 10, D and E). In addition, we found pools of small keratinocyte vesicles surround a stubby spine-like structure (Fig. 10 E and Fig. S5 B).

Discussion

Through its dendritic arbor, one melanocyte physically interacts with multiple keratinocytes across different layers of the epidermis. How melanocytes conduct and process communication with multiple cells is not understood. Other neural crest–derived cell types with branched cell morphologies are capable of receiving and processing information from neighboring cells at a local level, due, in part, to their cell shape and local biochemical activities including local release of signaling molecules, local receptors, and local elements, such as increases of cytosolic Ca^{2+} that amplify the response (Llinás and Hess, 1976; Llinás et al., 1968; Spencer and Kandel, 1961; Yuste and Denk, 1995). We investigated how melanocyte dendrites interact with neighboring keratinocytes using both an in vitro co-culture system and ultrastructure imaging of intact human skin. Our findings show that melanocytes produce compartmentalized fluctuations of Ca^{2+} in response to local signals from neighboring keratinocytes.

We found that keratinocytes also have small cytoplasmic projections both in situ and in culture, which contacted the melanocytes (Fig. 2). Similar structures were first described in amphibian skin at keratinocyte–keratinocyte junctions (Farquhar and Palade, 1965) and have been referred to as microvilli by other groups when discussing phagocytic events in keratinocytes (Ando et al., 2012). However, not much is known about their function or molecular composition, and it remains to be determined what class of cell extension they belong. The keratinocyte processes we observed wrapped around individual melanocyte dendrites (Fig. 2, A and D) and could be physically separating adjacent dendrites (Fig. 2 E). This local arrangement is similar to that of glial cells of the nervous system (Auld and Robitaille, 2003; Chong et al., 1999). Thus, keratinocyte projections may serve similar functions such as physically supporting the architecture of the melanocyte network across the skin as well as maintaining local signaling niches.

Endothelin and ACh secreted by keratinocytes elicited a localized Ca^{2+} response in melanocyte dendrites. Within the context of a multicellular tissue, the physical envelopment of melanocyte dendrites by the keratinocyte projections could facilitate localized delivery and recycling of secreted factors, similar to what occurs between cells of the nervous system (Auld and Robitaille, 2003; Chung et al., 2015). Further investigation into the molecular components of the keratinocyte projections

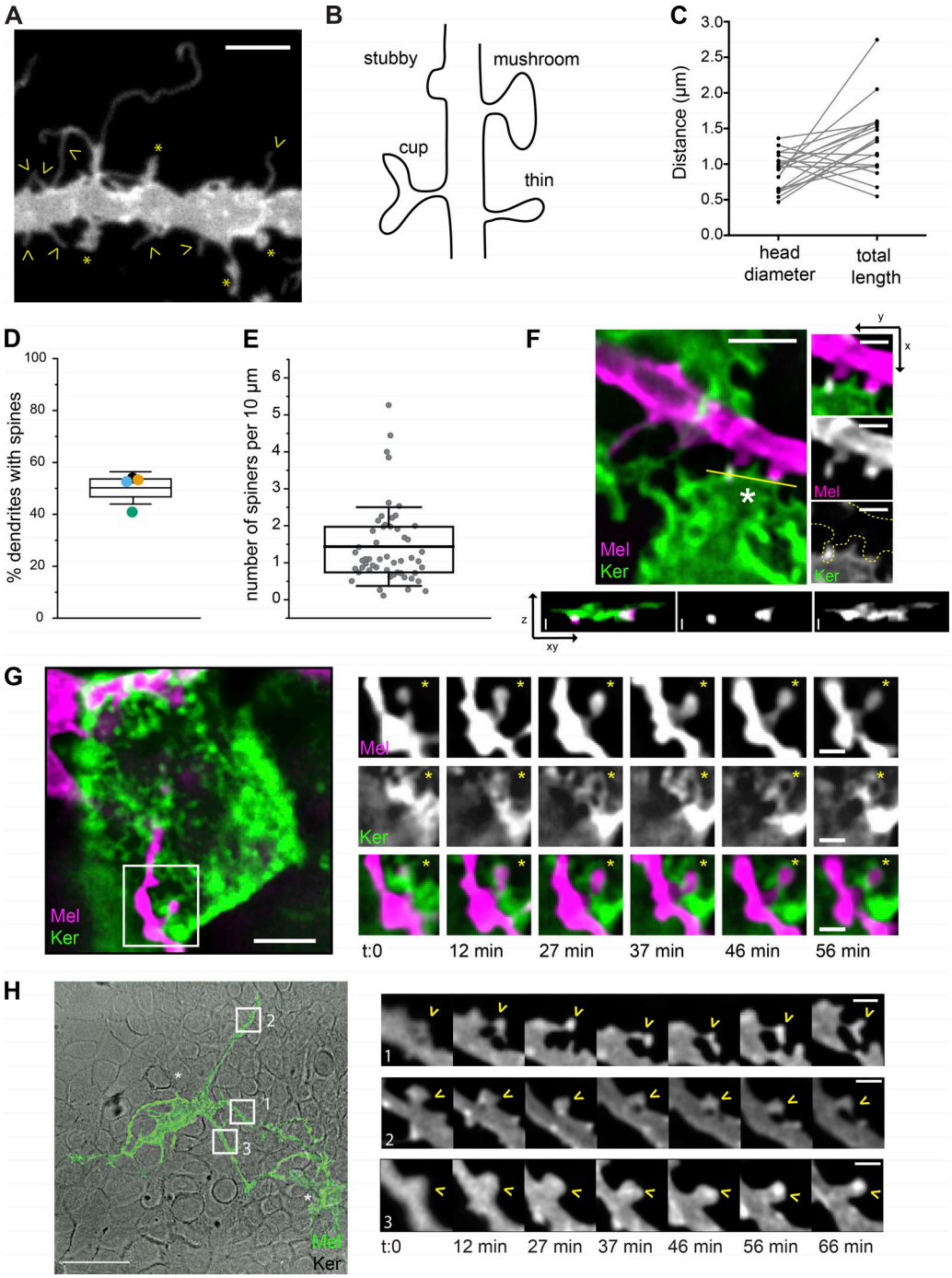

Figure 8. **Co-cultured melanocytes have dendritic spine-like structures. (A)** Representative image of dendritic spine-like structures (*) and filopodia (arrowheads) on co-cultured melanocyte expressing iRFPmem. **(B)** Illustration of spine-like structure shapes observed on co-cultured melanocyte dendrites. **(C)** Dimensions of spine-like structure head diameter and length. *n* = 20 total spine-like structures from four different skin donor derived co-cultures. **(D)** Percent of melanocyte dendrites with spine-like structures. *n* = 53 total dendrites from four co-cultures derived from different skin donors. Whiskers: 1 SD; box: 25–75%, mean. **(E)** The density of melanocyte dendritic spine-like structures vary from dendrite to dendrite. Whiskers: 1 SD; box: 25–75%, mean. *n* = 52 total dendrites from five co-cultures derived from different skin donors. **(F)** Co-cultured keratinocyte (eGFPmem, ker) processes interact with melanocyte (iRFPmem, mel) spine-like structures. Top right: X,Y images from asterisk in left panel. Bottom: Z, XY image from solid line in top left panel. **(G and H)** Some melanocyte (Mel) dendritic spines (*) have stable morphologies while interacting with adjacent keratinocytes (Ker; G), while others exhibit dynamic reshaping (<; H). Scale bars, (A) 5 µm; (F) top left, 5 µm; top right, 2 µm; bottom z axis, 1.5 µm; (G) left, 5 µm; right, 1.5 µm; (H) left, 50 µm; right, 2 µm.

as well as the stability and time scale of their interactions with melanocyte dendrites would provide further insight into their function.

Dendritic processes in neurons have functional domains and compartments that allow for local response and processing of cell–cell signaling events through compartmentalized changes of

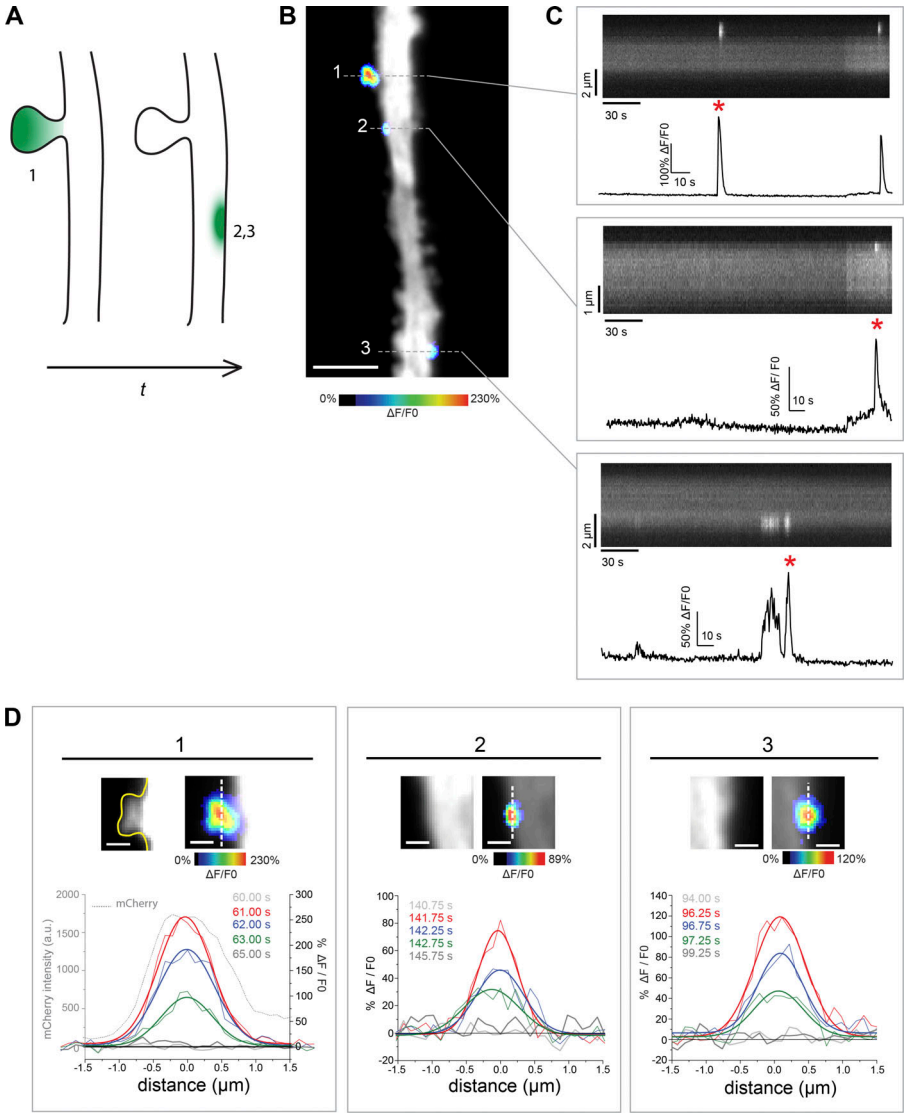

Figure 9. **Melanocyte dendritic spine-like structures compartmentalize Ca^{2+} transients. (A)** Schematic of confined Ca^{2+} transients (green) in dendritic spine-like structure and near the surface of melanocyte dendrites. See also Videos 6 and 7. **(B)** Dendrite from melanocyte expressing cytosolic mCherry and GCaMP6f in optimized co-culture with Ca^{2+} transients in a spine (1) and confined regions of the dendrite (2, 3). **(C)** Kymographs of GCaMP6f fluorescence signal, from the lines drawn through each of the three regions in B and the corresponding ΔF/F0 plot from a single ROI at the center of the signal. **(D)** Spread of Ca^{2+} signal (full width half maximum Gaussian fit, thick lines; raw data, thin lines) within the region (dashed line) for each location at the six indicated times corresponding to the peak marked with an asterisk in C. Region 1 has cytosolic mCherry signal indicating the physical boundaries of the spine. Scale bars, (B) 5 µm; (D) 1 µm.

cytoplasmic Ca^{2+} in the presynaptic terminal, post-synaptic dendritic spine, and/or dendrite (Katz and Miledi, 1965; Llinás et al., 1968, 1972; Llinás and Hess, 1976; Simon and Llinás, 1985; Spencer and Kandel, 1961; Yuste and Denk, 1995). Cytoplasmic fluctuations of Ca^{2+} within dendrites and dendritic spines regulate a variety of neuronal functions including local synaptic signaling, plasticity, protein translation as well as distal events such as gene transcription (Higley and Sabatini, 2008; Nimchinsky et al., 2002). Astrocytes can also respond to cell–cell signaling transmitters with transient compartmentalized increases of Ca^{2+} within their dendritic processes (Di Castro et al., 2011; Panatier et al., 2011). This type of localized cell–cell communication has been viewed as a hallmark of the nervous system. Dendritic morphologies are not unique to the nervous system, but it is not known if nonneuronal dendrites, such as those on melanocytes, are also capable of compartmentalizing signals received from adjacent cells. Previous work has demonstrated that Ca^{2+} concentration increases within the cell bodies of melanocytes in response to the exogenous addition of keratinocyte-derived paracrine factors (Imokawa et al., 1997; Kang et al., 1998). Here we show that Ca^{2+} transients originated from distinct regions within the melanocyte dendrite when they are co-cultured with keratinocytes. Similar Ca^{2+} transients are seen in the melanocyte dendrites and spines with the addition of ET-1 and ACh (Fig. 7, Fig. S3, and Fig. S4). These data are indicative of functional domains along melanocyte dendrites in which receptors and linked signaling cascades are restricted to, or active at, specific regions of the dendrite. The observed spatial distribution of localized Ca^{2+} transients could be the consequence of, but not limited to, Ca^{2+} buffering proteins, ER Ca^{2+} availability, and spatial distribution of IP3 receptors, as well as store operated calcium and calcium-induced calcium response machinery. Indeed, the spread of the Ca^{2+} response over a 14–22-µm (Fig. 3 H) length across the dendrites resembles the inositol-1,4,5-trisphosphate receptor-mediated dendritic Ca^{2+} transients previously described in pyramidal neurons and Purkinje cells (Finch and Augustine, 1998; Fitzpatrick et al., 2009; Manita and Ross, 2009).

ET-1 modulates, in a dose-dependent manner, melanogenesis, mRNA transcription, and proliferation of melanocytes in

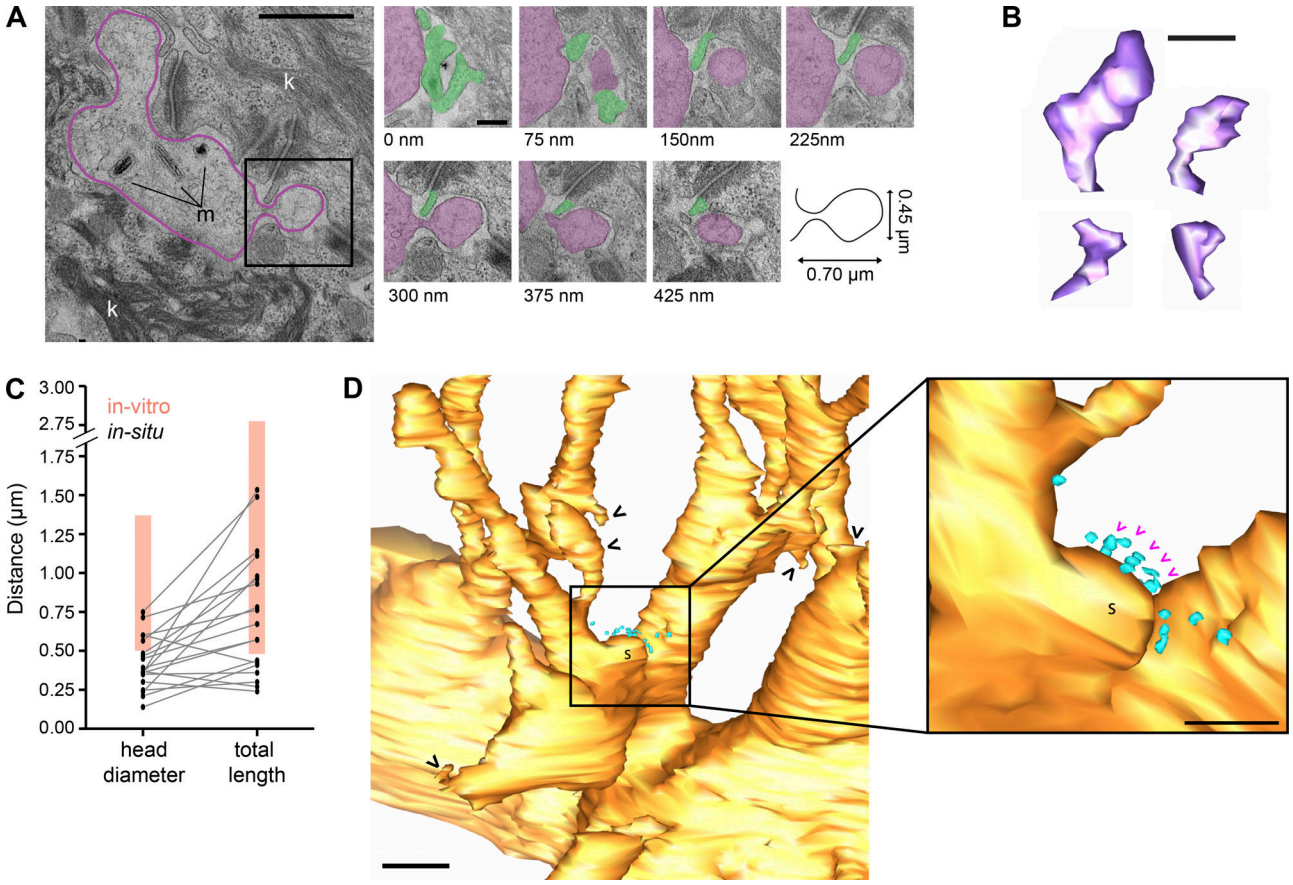

Figure 10. **Melanocytes within human skin have dendritic spine-like structures. (A)** Serial section TEM of a melanocyte dendritic spine-like structure in intact neonatal foreskin. Melanocyte dendrite highlighted in purple: m, melanosome; k, keratinocyte; keratinocyte processes highlighted in green. See also Fig. S4 A. **(B)** Dendritic spine-like structures from reconstructed melanocytes in the 3D FIB-SEM model are similar in shape and (C) size (n = 19, from four cells) to those in culture. Orange bars represent the distribution range from co-cultured (in vitro) spines. **(D)** Pooled vesicles in keratinocyte adjacent to melanocyte stubby shaped dendritic spine-like structure (s). Black arrowhead: spine-like structures; magenta arrowhead: vesicles in Fig. S4 B. Scale bars, (A) 1 µm; serial sections, 0.25 µm; (B) 5 µm; (C) 0.5 µm; (E) 5 µm; inset, 0.5 µm.

mono-culture (Imokawa et al., 1997; Imokawa et al., 1995; Tada et al., 1998). While transcription of mRNA and cell proliferation require transduction of signals into the nucleus, melanogenesis can be regulated locally (within dendrites) or globally (throughout the entire cell). Local regulation is achieved through alterations in the activity of melanin-synthesizing enzymes on melanosomes, whereas global regulation occurs through changes in the amount of melanosome-specific proteins. ET-1 has been shown to both up-regulate activity of tyrosinase, a key enzyme in melanin synthesis, and increase tyrosinase mRNA transcription in melanocytes (Imokawa et al., 1997). The ability to threshold a response to stimulus, such as local versus global Ca^{2+} increases, offers a possible mechanism by which melanocytes can regulate such outcomes. Previous work (Higley and Sabatini, 2008; Nimchinsky et al., 2002) has shown that compartmentalization of second messengers allows for spatial control of biochemical response to external stimuli that provide the cell a mechanism for local regulation of a variety of processes including protein translation, enzymatic activation, and recruitment of membrane receptors. We show that 10 nM ET-1 elicits a strong global change in cytosolic Ca^{2+} within seconds after application (Fig. 6 A, Fig. S3, and Video 3). However, in co-cultures without exogenous addition of ET-1, melanocytes have discrete dendritic transients in response to physiological levels of ET-1 secretion from neighboring keratinocytes (Fig. 3 B, Fig. 4, and Video 1) that are rapidly blocked by antagonists, suggesting an active signaling rather than a slow modulatory effect on transcription. These effects are at a much faster time scale than the previously described work showing global changes in melanocytes, such as transcriptional change, when melanocytes were incubated with 10 nM ET-1 for one or more days (Imokawa et al., 1997).

It should be noted that inhibition of the receptors for endothelin and ACh did not completely eliminate the number of melanocytes with dendritic Ca^{2+} transients in co-culture with keratinocytes (Fig. 7 E). The remaining Ca^{2+} transients in the melanocytes could be the result of other keratinocyte-derived factors or melanocyte autocrine factors or intrinsic signaling. While melanocytes in mono-culture did have a some dendritic Ca^{2+} transients, they were significantly fewer than those in co-culture (Fig. 3 G) and were often below the level seen in the co-cultures in the presence of antagonists of the ET-1 (BQ788) and ACh (atropine) (Fig. 7 E). This suggests there may be an additional secreted factor contributing to the dendritic Ca^{2+} transients in the melanocytes.

Last, we found dendritic spine-like structures on melanocytes in co-culture and in intact human skin. The morphology of the spine-like structures was strikingly similar to what has been described for neuronal dendritic spines (Nimchinsky et al., 2002; Stuart et al., 2007; Papa et al., 1995). While some spines were stable, others underwent morphological changes over time, similar to dendritic spines in neurons of live mice (Berning et al., 2012). We also observed that they were capable of compartmentalizing Ca^{2+}, another feature of neuronal dendritic spines. Neuronal dendritic spines are dynamic structures involved in short- and long-term plasticity at synapses. They can provide spatial restriction of cell–cell signaling that is disseminated throughout the cell upon receiving input that surpasses a threshold limit. It is possible that the dendritic spine-like structures on melanocyte dendrites function to integrate signals that determine the states of melanin production while providing a way to adapt to long-term responses to UV radiation. While further work is needed to determine if melanocyte dendritic spine-like structures are involved in cell–cell signaling, the presence of these physical structures on melanocytes provides an opportunity to understand the function and signaling mechanisms in such structures outside of the nervous system.

Materials and methods

Primary cell isolation

Melanocytes and keratinocytes were isolated as previously described (Picot, 2005) from neonatal foreskins obtained after routine circumcision, provided by Mount Sinai School of Medicine, New York, NY, or Weill Cornell Medical College, New York, NY, in accordance with the Rockefeller University Institutional Review Board protocol RBE-0721. Tissue was kept in CO_2 Independent Media (Gibco–Thermo Fisher Scientific) with 1× Antibiotic-Antimycotic (Gibco) at 4°C until processed for cell culture. In short, the epidermis was removed from the dermis via 10 mg/ml dispase II, neutral protease, grade II (Roche–Sigma-Aldrich), digestion for 14–17 h at 4°C. Single-cell suspension was achieved by mincing the epidermis and digesting with 0.5% trypsin (Gibco) for 5 min at 37°C. Trypsin was deactivated with soybean trypsin inhibitor (Gibco), and the cells were washed with Hanks' balanced salt solution, no Mg^{2+}, no Ca^{2+} (Gibco), before plating. Cells were grown at 37°C, in 5% CO_2 with 1× Antibioltic-Antimycotic. After the first media replacement, all antibiotics and antifungals were omitted from the growth media.

Cell culture

Melanocytes and keratinocytes were grown in melanocyte growth media (Medium 254 with Human Melanocyte Grow Serum-2; Gibco) and keratinocyte growth media (Epilife with Human Keratinocyte Growth Serum; Gibco), respectively. Only cells with five passages or fewer were used for experiments. 293T-HEK cells were grown in DMEM, high glucose, and pyruvate media (Gibco) supplemented with nonessential amino acids (Gibco) and 10% FBS at 37°C, 5% CO_2.

Optimized melanocyte–keratinocyte co-culture system

For melanocyte–keratinocyte co-cultures, melanocytes and keratinocytes were seeded at a 1:10 ratio (0.5×10^4:5×10^4 cells) onto the 10-mm glass window of a 35-mm MatTek dish (P35G-1.5-10-C, MatTek) in keratinocyte growth media (EpiLife media with Human Keratinocyte Growth Serum) and incubated 12–24 h at 37°C, 5% CO_2. Once a confluent monolayer was achieved, the media were changed to keratinocyte growth media containing 1.06 mM $CaCl_2$ final concentration. Subsequent experiments were performed 48–72 h after switching to 1.06 mM $CaCl_2$ media.

Immunofluorescence

Frozen sections

Within 12 h after harvest, neonatal foreskin (kept at 4°C in DMEM, high glucose, no pyruvate [Gibco] and Antibiotic-Antimytotic or CO_2 Independent media [Gibco] and Antibiotic-Antimytotic) was fixed overnight at 4°C with 4% paraformaldehyde (Electron Microscopy Sciences). After washing with PBS, the fixed tissue was incubated with 30% sucrose in DPBS overnight at 4°C. The sucrose was exchanged with Optimal Cutting Temperature OCT compound (VWR) and frozen on dry ice. In Fig. S1 B, a cryostat section of ∼5–10 µm was used. After immunofluorescence, the section was mounted in ProLong Gold (Molecular Probes) and sealed.

Epidermal sheets

For Fig. S1, the epidermis was removed from the dermis by overnight incubation with dispase II. Freshly isolated epidermal sheets were fixed with 4% paraformaldehyde overnight at 4°C and washed before immunofluorescence staining. Epidermal sheets were imaged in PBS rather than mounting media to prevent compaction of tissue and loss of z resolution.

Cell cultures

Cell cultures were washed 1× with PBS, fixed in 4% paraformaldehyde for 10–30 min at room temperature, and then washed before immunofluorescence staining.

After fixation, tissue (either fixed frozen sections or epidermal sheets) or cells were incubated in blocking buffer: 2.5% donkey serum, 2.5% goat serum (Jackson ImmunoResearch Laboratories), 1% bovine serum albumin (Sigma-Aldrich), and 0.1% Triton X-100 (Sigma-Aldrich) for 1–2 h at room temperature. The following primary antibodies were used at the indicated concentration in blocking buffer overnight at 4°C: mouse monoclonal anti-TRP1 1:200 (TA99, ab3312, Abcam), mouse monoclonal anti-K14 1:300 (LL002, ab7800), mouse monoclonal anti-E cadherin 1:100 (ab1416, Abcam), rabbit monoclonal anti-β catenin 1:100 (8480T, Cell Signaling Technology), mouse monoclonal anti-PCAD 1:100 (MAB861, R&D Systems), mouse monoclonal anti-cKit 1:100 (CD11705, Invitrogen–Thermo Fisher Scientific), rabbit polyclonal anti-K10 1:500 (Poly19054, BioLegendA), and rat monocolonal anti-α6 integrin (eBioGoH3 [GoH3], Invitrogen–Thermo Fisher Scientific). Secondary antibodies against mouse IgG, rat IgG, or rabbit IgG conjugated to Alexa Fluor 488, 594, or 680 (Molecular Probes–Thermo Fisher Scientific) were used at a 1:1,000 dilution for 1–2 h at room temperature. Hoechst (Molecular Probes) was used at a 1:1,000 dilution in PBS. Secondary antibodies against mouse IgG2a and mouse IgG1 were used for dual staining of PCAD and TRP1, ECAD

and TRP1, and the two-color double anti-TRP1 and anti-cKit immunofluorescence (Fig. S1 A). For all other TRP1/cKit staining, a pan anti-mouse IgG was used to detect both primary antibodies.

Microinjections

Freshly isolated neonatal foreskin epidermis was obtained by an overnight dispase digestion at 4°C and removal from the dermis while on ice. Individual melanocytes were microinjected using a manual microinjection (model MM-88-0, Narashige International) system on an Upright BX61WI microscope with manual syringe pressure application. 2% (wt/vol) Lucifer yellow CH, Lithium Salt (Molecular Probes) was directly injected into the basal surface of the melanocyte at room temperature.

EM

FIB-SEM

Neonatal foreskin was immersion fixed in 4% paraformaldehyde, 2% glutaraldehyde, 2 mM $CaCl_2$, and 0.1 M sodium cacodylate at 4°C. Tissue was cut into 1-mm × 500-µm pieces for processing. Tissue was then post-fixed with 2% osmium tetroxide and 1.5% potassium ferrocyanide on ice for 1 h followed by a thiocarbohydrazide amplification step for 20 min and then a subsequent 2% osmium tetroxide incubation for 30 min at room temperature. Tissue was then stained with 1% uranyl acetate overnight at 4°C. Lead aspartate staining was performed for 30 min at 60°C the next day followed by tissue dehydration using sequential ethanol dehydration followed by propylene oxide and embedded in Durcapan resin (Sigma-Aldrich). The sample block was trimmed then mounted on a SEM sample holder using double-sided carbon tape (EMS). Colloidal silver paint (EMS) was used to electrically ground the exposed edges of the tissue block. The entire surface of the specimen was then sputter coated with a thin layer of gold/palladium. The tissue was imaged using back scattered electron mode in a FEI Helios Nanolab 650. Images were recorded after each round of ion beam milling using the SEM beam at 2 keV and 100 pA with a working distance of 2.8 mm. Data acquisition occurred in an automated way using the Auto Slice and View G3 software. The raw images were 2,048 × 1,768 pixels, with 30-nm slices viewed at a −38° cross-sectional angle. Each raw image had a horizontal field width of 30 µm with an XY pixel size of 14–18 nm and 30-nm Z slices. These images were then aligned using the image processing programs in IMOD (Kremer et al., 1996). The aligned images were then use to generate a 3D model in IMOD's 3dmod image display and modeling program.

TEM serial sections

Neonatal foreskin was immersion-fixed in 4% paraformaldehyde, 2% glutaraldehyde, 2 mM $CaCl_2$, and 0.1 M sodium cacodylate at 4°C. Tissue was cut into 1-mm × 500-µm pieces for processing. Tissue was post-fixed with 1% osmium tetroxide on ice for 3 h followed by uranyl acetate staining (1% in 0.05 M maleate buffer, pH 5.2) overnight at 4°C. The next day, tissue was dehydrated using sequential ethanol dehydration followed by propylene oxide and embedded in epon resin (Electron Microscopy Sciences). "Gray sections" for TEM (~50–100-nm sections) were used. Sections were imaged on a JEM 100CX Transmission Electron Microscope (JEOL USA) with an AMT 2K × 2K digital camera at the Rockefeller University Electron Microscopy Resource Center.

Keratinocyte–melanocyte contact dependence assay

To assess the percent of melanocytes with transients in co-culture and mono-culture conditions, all cultures were seeded onto the 10-mm glass window of a collagen I–coated MatTek dish. The following seeding ratios and growth media were used: "10× ker" is 0.5×10^4 melanocytes expressing GCaMP6f (mel6f) and 5×10^4 keratinocytes, grown in keratinocyte growth media; "Mel alone" is 0.5×10^4 mel6f grown in melanocyte media; "10× Mel" is 0.5×10^4 mel6f and 5×10^4 nontransduced melanocytes in melanocyte media; "10× 293T" is 0.5×10^4 mel6f and 5×10^4 HEK293T cells; and "TW" is 0.5×10^4 mel6f seeded on the glass bottom of a collagen I–coated MatTek dish with 5×10^4 keratinocytes seeded into a collagen I–coated Transwell culture insert, 3 µm pore (CORNING), above the glass window, grown in keratinocyte media. For all culture conditions, cultures were incubated overnight at 37°C, 5% CO_2, and media were replaced with fresh media containing 1.06 mM $CaCl_2$. Cultures were imaged 48 h after media change. To compare the effect of different growth conditions for co-cultures and mono-cultures, 10× Ker, Mel alone, 10× Mel, 10× 293T, and TW 10× Ker were grown in triplicate with one dish for each media condition: keratinocyte media, melanocyte media, and 50/50 media (1:1 melanocyte: keratinocyte media). Keratinocyte-conditioned media were obtained by harvesting the supernatant from a skin donor–matched keratinocyte culture at each step of the culturing process mentioned above.

Image acquisition and quantification

Immunofluorescence

Images were acquired using cellSens software (Olympus) on an IX83 microscope (Olympus) with a UPLSAPO 60× 1.3 NA silicone oil objective (Olympus) and an Orca-ER CCD digital camera (Hamamatsu Photonics). Deconvolution was done with Autoquant (Media Cybernetics) standard settings for each filter set using a blind adaptive point-spread function. Image analysis was done in Fiji (http://fiji.sc/).

Cell cultures

Cultures in MatTek dishes were imaged (fluorescence and infrared–differential interference contrast) on an Upright BX61WI microscope (Olympus) with a UMPlan FL 60× 1.0 NA water dipping objective (Olympus), an Orca Flash 4.0 digital CMOS camera (Hamamatsu) using MetaMorph image acquisition software (Molecular Devices), or a DeltaVision system (GE Healthcare) at the Rockefeller University Bio-Imaging Resource Center with a 60× NA 1.52 oil objective and SoftWoRx software (DeltaVision). Deconvolution was performed using the adaptive point spread setting in Autoquant (Media Cybernetics) or, for images acquired on the DeltaVision, deconvolution was performed using the measured point-spread function in the SoftWoRx software. All imaging was conducted at room temperature. Image analysis as described below was done in Fiji.

Ca^{2+} imaging

Cultures were imaged in a modified DPBS (10 mM Hepes, 10 mM D-glucose, 0.1 µM glycine, 1.06 mM $CaCl_2$, and 0.5 mM $MgCl_2$, pH 7.1–7.3) without exogenous growth factors. Exceptions were Ca^{2+} source, agonist, and antagonist assays, which are described below. Prior to imaging, melanocyte–keratinocyte co-cultures were washed 3× with modified DPBS. Cultures were imaged in streaming acquisition mode in Metamorph Software (Molecular Devices) with a 250-ms exposure time on the Upright BX61WI microscope at room temperature using UMPlan FL 10×, 0.3 NA water dipping objective, or UMPlan FL 60×, 1.0 NA water dipping objective. GCaMP6f was used to measure relative cytosolic Ca^{2+} levels for all Ca^{2+} imaging experiments except for co-cultures, where keratinocytes were infected with EDN1 or CHAT shRNA. Darmacon GIPZ shRNA lentivectors contain turboGFP, and therefore we could not use the green calcium reporter GCaMP6f in melanocytes. Instead, a red calcium reporter, RCaMP1h, was used.

Number of cells with transients was quantified by manually counting the cells with at least one transient Ca^{2+} signal during the 2.5-min imaging period. For each positive cell, presence of local or global Ca^{2+} transients was manually determined.

Number of transients per cell was quantified by manually counting individual peaks in fluorescence by eye using line scans along the dendrite, or a region of interest (ROI) was drawn at initiation sight and a plot of the fluorescence intensity over time was used to determine the number of peaks and thus the number of transients. It should be noted that the use of a 0.3-NA, 10× objective limited the analysis to the brightest fluorescence signals, and therefore our final count is likely an underestimate of the frequency.

Spatiotemporal assessment of transients was done on images acquired in streaming mode with 50 ms or 250 ms exposure using a UMPlan FL 60×, 1.0 NA, water dipping objective. The distribution of the spread in Ca^{2+} signal was determined using data acquired in streaming mode with a 250-ms exposure time using a UMPlan FL 10×, 0.3 NA water dipping objective.

For calculating ΔF/F0, F0 was determined by averaging 10 consecutive fluorescence intensities, within the same ROI, at the lowest fluorescence intensity point during the imaging sequence. ΔF was determining by: ΔF = Fn − F0, where Fn is the fluorescence intensity at that given time point. For ΔF/F0 images, 10 consecutive frames were averaged, and the resulting image was used as F0. The ΔF image was obtained by subtracting the F0 image from the frame corresponding to the peak Ca^{2+} signal in the corresponding ΔF/F0 plot. The final ΔF/F0 image was obtained by dividing the ΔF image by the F0 image.

Ca^{2+} source, agonist, and antagonist assays

Co-cultures in modified DPBS, 1.06 mM $CaCl_2$, were imaged for 2.5 min in streaming mode, 250 ms exposure, to determine the baseline percentage of cells with transients and the number of transients per cell. After baseline imaging, media were replaced with modified DPBS, containing 0 mM $CaCl_2$ and/or 1 µM thapsigargin, 1 µM BQ788, 1 µM BQ123 (Tocris–BioTechne), 100 µM atropine sulfate (Sigma-Aldrich), or 100 µM atropine sulfate with 1 µM BQ788. To ensure full replacement of the imaging media with the treatment solution, 10 times the volume of the imaging chamber was perfused through the imaging chamber of a MatTek dish using manual syringe-driven delivery through a modified open perfusion insert (model RC-37F; Warner Instruments). The same field of view imaged for the baseline analysis was imaged after a 20-min incubation with the perfused solution. The fold change in percent melanocytes with one or more Ca^{2+} transients was determined by dividing the number of cells with transients during the treatment imaging period by the number of cells with transients during the baseline imaging period. For agonist stimulation, ACh chloride (Tocris) or endothelin-1 acetate salt (Bachem) was perfused into the chamber at 10× excess volume, to ensure complete replacement of imaging media, at the indicated time during the streaming acquisition.

Lentiviral vectors and production

Phi3-EGFPmem

EGFPmem was made by replacing ECFP with EGFP in the Clontech vector pECFPmem (Clontech–Takara Bio USA). EGFPmem was inserted into the HIV-1–based lentivirus vector pLVX Phi3 (Takacs et al., 2017a) using restriction enzymes BamHI and XbaI and Quick Ligation Kit (New England BioLabs).

Phi3-iRFPmem

Annealed sense and antisense DNA oligos containing the sequence for the first 20 amino acids of neuromodulin (mem) flanked by 5′ XhoI and 3′ NotI restriction enzyme sites were inserted into pLVX Phi3 by restriction digest and subsequent ligation using the Quick Ligation Kit (New England BioLabs). Near-infrared fluorescent protein (iRFP; Filonov et al., 2011) was PCR-amplified from the plasmid piRFP (a gift from V. Verkhusha, Addgene plasmid 31857; http://n2t.net/addgene:31857; RRID:Addgene_31857) using forward primer: 5′-CAAAAGATC GCGGCCGAAGGATCTGTCGCCAGG-3′, reverse primer: 5′-GCG TCCGGAGCGGCCTTACTCTTCCATCACGCCG-3′, and then inserted into the NotI-digested Phi3-mem plasmid after the neuromodulin plasma membrane binding domain using the In-Fusion HD Cloning Kit (Clonetech).

Zhi3-mCherry

mCherry (from pmCherry-N1; Clonetech) was inserted in PLVX Zhi3 (Takacs et al., 2017b) using restriction enzymes MluI and BamHI and a Quick Ligation Kit (New England Biolabs).

Phi3-GCaMP6f

GCaMP6f from pGP-CMV-GCaMP6f (a gift from D. Kim) was excised from Addgene plasmid 40753 using restriction enzymes BglII and XbaI and inserted into BamHI- and XbaI-digested PLVX Phi3 (Takacs et al., 2017a) using the Quick Ligation Kit.

Phi3-RCaMP1h

RCaMPh1 was amplified from pRSET-RCaMP1h, a gift from L. Looger (Addgene plasmid 42874; http://n2t.net/addgene:42874; RRID: Addgene_42874), using forward primer: 5′-TAGATCTCGAGAATT GCCACCATGGGTTCTCATCATCATCA-3′, reverse primer: 5′-GAG CGGCCGCGAATTTTACTTCGCTGTCATCATTTG-3′ and inserted

into ECoRI-digested PLVX Phi3 using Cold Fusion ligation independent cloning (Systems Bioscience).

Low-passage HEK293T cells (60–80% confluent) were co-transfected using polyethyleneimine (Sigma-Aldrich) at a 5:5:1 ratio of a lentiviral plasmid, a HIV-1 GagPol plasmid, and a VSVg plasmid, respectively. To obtain viral stocks, 88 µg of total DNA was used to transfect a 150-mm dish of 70% confluent cells. Virus-producing HEK293Ts were maintained in DMEM, high glucose, pyruvate media (Gibco) supplemented with nonessential amino acids (Gibco) and 3% FBS (Sigma-Aldrich). Virus-containing media were collected at 24 h, 48 h, and 72 h after transfection, filtered through a 0.45-µm filter (EMD Millipore), and concentrated with Lenti-X Concentrator (Clontech). Concentrated virus was resuspended in Hanks' balanced salt solution or phosphate buffered saline and stored in aliquots at 20× final concentration. High titer virus stocks were stored at −86°C for future use.

DsiRNA knockdown

DsiRNAs were generated from DsiRNA sequences predesigned by IDT (Integrated DNA Technologies). Duplexed sequences were as follows: EDNRA 13.1 antisense: 5′-GGACAAGAACCGAUGUGAAUUACTT-3′, sense: 5′-AAGUAAUUCACAUCGGUUCUUGUCCAU-3′, EDNRA 13.2 antisense: 5′-GCAACCUUCUGCAUUCAUAAAUCTT-3′, sense: 5′-AAGAUUUAUGAAUGCAGAAGGUUGCUA-3′, EDNRB 13.1 antisense: 5′-CAUGUCAGUAUCAUGUUCUCUAATT-3′, sense: 5′-AAUUAGAGAACAUGAUACUGACAUGGA-3′, EDNRB 13.2 antisense: 5′-AGUAUUGACAGAUAUCGAGCUGUTG-3′, sense: 5′-CAACAGCUCGAUAUCUGUCAAUACUCA-3′.

On day 0, DsiRNA were introduced to melanocytes using Lipfectamine RNAiMAX transfection reagent (Invitrogen–Thermo Fisher Scientific), following the recommended transfection procedure for 35-mm dishes. On day 1, melanocytes were infected with Phi3-GCaMP6f and incubated overnight. On day 2, melanocytes were seeded with keratinocytes to generate co-cultures as described above.

shRNA knockdown

Knockdown of CHAT and EDN1 was achieved through transduction of keratinocytes with the GIPZ shRNAs EDN1: V3LHS_151308, V3LHS_370736, V3LHS_370739 CHAT: V3LHS_393516, V3LHS_393518. Keratinocytes were grown for 48 h after transduction and then underwent bulk selection using 2 µg/ml puromycin for 48 h. Cultures were maintained in 1 µg/ml puromycin until seeded for co-cultures.

RNA extraction, cDNA synthesis, and quatitative RT-PCT (qRT-PCR)

Keratinocytes were harvested in 1 ml TRIzol Reagent (Invitrogen–Thermo Fisher Scientific), and RNA was purified following the manufacturer's protocol. cDNA synthesis was done using the SensiFAST cDNA Synthesis kit (Bioline) according to the manufacturer's protocol. Subsequent qRT-PCR was performed using SensiFAST SYBER NO-ROX Kit, with the manufacturer's suggested two-step protocol using the follow primers for EDN1: forward 5′-CAGAAACAGCAGTCTTAGGCG-3′, reverse 5′-GTCCAGGTGGCAGAAGTAGAC-3′; CHAT: forward 5′-CGGTCCTCGTGAAAGACTCC-3′, reverse 5′-GGACTTGTCGTACCAGCGAT-3′; housekeeping gene GPI for internal normalization: forward 5′-CCAACAAGGACCGCTTCAAC-3′, reverse 5′-CATCACGTCCTCCGTCACC-3′.

Statistical analysis

Two-sample *t* test, one-way ANOVA with Tukey means comparison, and Kruskal–Wallis ANOVA statistical analyses were performed using standard settings in OriginPro software (OriginLab) as indicated in the figure legends and main text. We used the customary threshold of $P < 0.05$ to declare statistical significance. Sample size and statistical details can be found in the figures, legends, and main text.

Online supplemental material

Fig. S1 shows melanocyte morphology in intact neonatal foreskin. Fig. S2 shows that growth media do not influence the percent of melanocytes with dendritic Ca^{2+} transients. Fig. S3 shows melanocyte response to exogenous ET-1 in co-cultures and mono-cultures. Fig. S4 shows melanocyte response to exogenous ACh in co-cultures and mono-cultures. Fig. S5 shows the ultrastructure of melanocyte dendritic spine-like structures and pooled vesicles in adjacent keratinocyte. Table S1 shows quantification of melanocyte dendrites and spines from FIB-SEM reconstruction. Video 1 shows Ca^{2+} transients in co-cultured melanocytes. Video 2 shows dendritic Ca^{2+} transients. Video 3 shows the co-cultured melanocyte response to exogenous 10 nM ET-1. Video 4 shows abrogation of Ca^{2+} transients in co-culture melanocytes in the presence of BQ788 but not BQ123. Video 5 shows co-cultured melanocyte response to exogenous ACh. Video 6 shows Ca^{2+} transients in a co-cultured melanocyte dendrite and dendritic spines. Video 7 shows Ca^{2+} transient in co-cultured melanocyte dendritic spines.

Acknowledgments

We thank the Departments of Obstetrics and Gynecology at Mt. Sinai School of Medicine and Cornell-Weill for their assistance in the collection of the neonatal foreskins. We thank the Rockefeller Electron Microscopy Resource Center, the Rockefeller University Bio-Imaging Resource Center, and the Simons Electron Microscopy Center for assistance. We thank Pascal Maguin for assistance with cloning and Marina Bleck, Constantin Takacs, Michelle Itano, Sohail Tavazoie, and Elaine Fuchs for helpful discussions.

The FIB-SEM data were acquired at the Simons Electron Microscopy Center and National Resource for Automated Molecular Microscopy located at the New York Structural Biology Center, supported by grants from the Simons Foundation (349247), NYSTAR, and the National Institutes of Health, National Institute of General Medical Sciences (GM103310), with additional support from National Institutes of Health grant S10 RR029300-01. This work was supported in part by a National Center for Advancing Translational Sciences grant (UL1 TR001866; National Institutes of Health Clinical and Translational Science Award program), National Institute of General Medical Sciences of the National Institutes of Health under

award T32GM066699, and a Rockefeller University Women in Science Fellowship to R.L. Belote.

The authors declare no competing financial interests.

Author contributions: R.L. Belote performed the experiments, and R.L. Belote and S.M. Simon designed the experiments and wrote the manuscript.

Submitted: 2 February 2019
Revised: 19 September 2019
Accepted: 25 October 2019

References

Adameyko, I., F. Lallemend, J.B. Aquino, J.A. Pereira, P. Topilko, T. Müller, N. Fritz, A. Beljajeva, M. Mochii, I. Liste, et al. 2009. Schwann cell precursors from nerve innervation are a cellular origin of melanocytes in skin. *Cell.* 139:366–379. https://doi.org/10.1016/j.cell.2009.07.049

Ando, H., Y. Niki, M. Ito, K. Akiyama, M.S. Matsui, D.B. Yarosh, and M. Ichihashi. 2012. Melanosomes are transferred from melanocytes to keratinocytes through the processes of packaging, release, uptake, and dispersion. *J. Invest. Dermatol.* 132:1222–1229. https://doi.org/10.1038/jid.2011.413

Auld, D.S., and R. Robitaille. 2003. Glial cells and neurotransmission: an inclusive view of synaptic function. *Neuron.* 40:389–400. https://doi.org/10.1016/S0896-6273(03)00607-X

Berning, S., K.I. Willig, H. Steffens, P. Dibaj, and S.W. Hell. 2012. Nanoscopy in a living mouse brain. *Science.* 335:551. https://doi.org/10.1126/science.1215369

Buchli, R., A. Ndoye, J. Arredondo, R.J. Webber, and S.A. Grando. 2001. Identification and characterization of muscarinic acetylcholine receptor subtypes expressed in human skin melanocytes. *Mol. Cell. Biochem.* 228:57–72. https://doi.org/10.1023/A:1013368509855

Chen, T.W., T.J. Wardill, Y. Sun, S.R. Pulver, S.L. Renninger, A. Baohan, E.R. Schreiter, R.A. Kerr, M.B. Orger, V. Jayaraman, et al. 2013. Ultrasensitive fluorescent proteins for imaging neuronal activity. *Nature.* 499:295–300. https://doi.org/10.1038/nature12354

Chong, M.S., C.J. Woolf, N.S. Haque, and P.N. Anderson. 1999. Axonal regeneration from injured dorsal roots into the spinal cord of adult rats. *J. Comp. Neurol.* 410:42–54. https://doi.org/10.1002/(SICI)1096-9861(19990719)410:1<42::AID-CNE5>3.0.CO;2-F

Chung, W.S., N.J. Allen, and C. Eroglu. 2015. Astrocytes Control Synapse Formation, Function, and Elimination. *Cold Spring Harb. Perspect. Biol.* 7:a020370. https://doi.org/10.1101/cshperspect.a020370

De Luca, M., A.T. Franzi, F. D'Anna, A. Zicca, E. Albanese, S. Bondanza, and R. Cancedda. 1988. Coculture of human keratinocytes and melanocytes: differentiated melanocytes are physiologically organized in the basal layer of the cultured epithelium. *Eur. J. Cell Biol.* 46:176–180.

Di Castro, M.A., J. Chuquet, N. Liaudet, K. Bhaukaurally, M. Santello, D. Bouvier, P. Tiret, and A. Volterra. 2011. Local Ca2+ detection and modulation of synaptic release by astrocytes. *Nat. Neurosci.* 14:1276–1284. https://doi.org/10.1038/nn.2929

Eberle, J., S. Weitmann, O. Thieck, H. Pech, M. Paul, and C.E. Orfanos. 1999. Downregulation of endothelin B receptor in human melanoma cell lines parallel to differentiation genes. *J. Invest. Dermatol.* 112:925–932. https://doi.org/10.1046/j.1523-1747.1999.00598.x

Erickson, C.A., T.D. Duong, and K.W. Tosney. 1992. Descriptive and experimental analysis of the dispersion of neural crest cells along the dorsolateral path and their entry into ectoderm in the chick embryo. *Dev. Biol.* 151:251–272. https://doi.org/10.1016/0012-1606(92)90231-5

Farquhar, M.G., and G.E. Palade. 1965. Cell junctions in amphibian skin. *J. Cell Biol.* 26:263–291. https://doi.org/10.1083/jcb.26.1.263

Filonov, G.S., K.D. Piatkevich, L.M. Ting, J. Zhang, K. Kim, and V.V. Verkhusha. 2011. Bright and stable near-infrared fluorescent protein for in vivo imaging. *Nat. Biotechnol.* 29:757–761. https://doi.org/10.1038/nbt.1918

Finch, E.A., and G.J. Augustine. 1998. Local calcium signalling by inositol-1,4,5-trisphosphate in Purkinje cell dendrites. *Nature.* 396:753–756. https://doi.org/10.1038/25541

Fitzpatrick, T.B., and A.S. Breathnach. 1963. [THE EPIDERMAL MELANIN UNIT SYSTEM]. *Dermatol. Wochenschr.* 147:481–489.

Fitzpatrick, T.B., and G. Szabo. 1959. The melanocyte: cytology and cytochemistry. *J. Invest. Dermatol.* 32:197–209. https://doi.org/10.1038/jid.1959.37

Fitzpatrick, J.S., A.M. Hagenston, D.N. Hertle, K.E. Gipson, L. Bertetto-D'Angelo, and M.F. Yeckel. 2009. Inositol-1,4,5-trisphosphate receptor-mediated Ca2+ waves in pyramidal neuron dendrites propagate through hot spots and cold spots. *J. Physiol.* 587:1439–1459. https://doi.org/10.1113/jphysiol.2009.168930

Gordon, P.R., C.P. Mansur, and B.A. Gilchrest. 1989. Regulation of human melanocyte growth, dendricity, and melanization by keratinocyte derived factors. *J. Invest. Dermatol.* 92:565–572. https://doi.org/10.1111/1523-1747.ep12709595

Grando, S.A., D.A. Kist, M. Qi, and M.V. Dahl. 1993. Human keratinocytes synthesize, secrete, and degrade acetylcholine. *J. Invest. Dermatol.* 101:32–36. https://doi.org/10.1111/1523-1747.ep12358588

Higley, M.J., and B.L. Sabatini. 2008. Calcium signaling in dendrites and spines: practical and functional considerations. *Neuron.* 59:902–913. https://doi.org/10.1016/j.neuron.2008.08.020

Hirobe, T. 2014. Keratinocytes regulate the function of melanocytes. *Dermatologica Sinica.* 32:200–204.

Imokawa, G., M. Miyagishi, and Y. Yada. 1995. Endothelin-1 as a new melanogen: coordinated expression of its gene and the tyrosinase gene in UVB-exposed human epidermis. *J. Invest. Dermatol.* 105:32–37. https://doi.org/10.1111/1523-1747.ep12312500

Imokawa, G., T. Kobayashi, M. Miyagishi, K. Higashi, and Y. Yada. 1997. The role of endothelin-1 in epidermal hyperpigmentation and signaling mechanisms of mitogenesis and melanogenesis. *Pigment Cell Res.* 10:218–228. https://doi.org/10.1111/j.1600-0749.1997.tb00488.x

Jimbow, K., W.C. Quevedo Jr., T.B. Fitzpatrick, and G. Szabo. 1976. Some aspects of melanin biology: 1950-1975. *J. Invest. Dermatol.* 67:72–89. https://doi.org/10.1111/1523-1747.ep12512500

Kang, H.Y., W.H. Kang, and C. Lee. 1998. Endothelin-B receptor-mediated Ca2+ signaling in human melanocytes. *Pflugers Arch.* 435:350–356.

Katz, B., and R. Miledi. 1965. The Effect of Calcium on Acetylcholine Release from Motor Nerve Terminals. *Proc. R. Soc. Lond. B Biol. Sci.* 161:496–503. https://doi.org/10.1098/rspb.1965.0017

Kremer, J.R., D.N. Mastronarde, and J.R. McIntosh. 1996. Computer visualization of three-dimensional image data using IMOD. *J. Struct. Biol.* 116:71–76. https://doi.org/10.1006/jsbi.1996.0013

Lei, T.C., V.M. Virador, W.D. Vieira, and V.J. Hearing. 2002. A melanocyte-keratinocyte coculture model to assess regulators of pigmentation in vitro. *Anal. Biochem.* 305:260–268. https://doi.org/10.1006/abio.2002.5665

Llinás, R., and R. Hess. 1976. Tetrodotoxin-resistant dendritic spikes in avian Purkinje cells. *Proc. Natl. Acad. Sci. USA.* 73:2520–2523. https://doi.org/10.1073/pnas.73.7.2520

Llinás, R., C. Nicholson, J.A. Freeman, and D.E. Hillman. 1968. Dendritic spikes and their inhibition in alligator Purkinje cells. *Science.* 160:1132–1135. https://doi.org/10.1126/science.160.3832.1132

Llinás, R., J.R. Blinks, and C. Nicholson. 1972. Calcium transient in presynaptic terminal of squid giant synapse: detection with aequorin. *Science.* 176:1127–1129. https://doi.org/10.1126/science.176.4039.1127

Lytton, J., M. Westlin, and M.R. Hanley. 1991. Thapsigargin inhibits the sarcoplasmic or endoplasmic reticulum Ca-ATPase family of calcium pumps. *J. Biol. Chem.* 266:17067–17071.

Manita, S., and W.N. Ross. 2009. Synaptic activation and membrane potential changes modulate the frequency of spontaneous elementary Ca2+ release events in the dendrites of pyramidal neurons. *J. Neurosci.* 29:7833–7845. https://doi.org/10.1523/JNEUROSCI.0573-09.2009

Marks, M.S., and M.C. Seabra. 2001. The melanosome: membrane dynamics in black and white. *Nat. Rev. Mol. Cell Biol.* 2:738–748. https://doi.org/10.1038/35096009

Nimchinsky, E.A., B.L. Sabatini, and K. Svoboda. 2002. Structure and function of dendritic spines. *Annu. Rev. Physiol.* 64:313–353. https://doi.org/10.1146/annurev.physiol.64.081501.160008

Panatier, A., J. Vallée, M. Haber, K.K. Murai, J.C. Lacaille, and R. Robitaille. 2011. Astrocytes are endogenous regulators of basal transmission at central synapses. *Cell.* 146:785–798. https://doi.org/10.1016/j.cell.2011.07.022

Papa, M., M.C. Bundman, V. Greenberger, and M. Segal. 1995. Morphological analysis of dendritic spine development in primary cultures of hippocampal neurons. *J. Neurosci.* 15:1–11. https://doi.org/10.1523/JNEUROSCI.15-01-00001.1995

Picot, J. 2005. Human cell culture protocols. Humana Press, Totowa, NJ. 359 pp.

Reid, K., A.M. Turnley, G.D. Maxwell, Y. Kurihara, H. Kurihara, P.F. Bartlett, and M. Murphy. 1996. Multiple roles for endothelin in melanocyte development: regulation of progenitor number and stimulation of differentiation. *Development.* 122:3911–3919.

Scott, G., S. Leopardi, S. Printup, and B.C. Madden. 2002. Filopodia are conduits for melanosome transfer to keratinocytes. *J. Cell Sci.* 115: 1441–1451.

Simon, S.M., and R.R. Llinás. 1985. Compartmentalization of the submembrane calcium activity during calcium influx and its significance in transmitter release. *Biophys. J.* 48:485–498. https://doi.org/10.1016/S0006-3495(85)83804-2

Singh, S.K., R. Kurfurst, C. Nizard, S. Schnebert, E. Perrier, and D.J. Tobin. 2010. Melanin transfer in human skin cells is mediated by filopodia--a model for homotypic and heterotypic lysosome-related organelle transfer. *FASEB J.* 24:3756–3769. https://doi.org/10.1096/fj.10-159046

Spencer, W.A., and E.R. Kandel. 1961. Electrophysiology of Hippocampal Neurons: Iv. Fast Prepotentials. *J. Neurophysiol.* 24:272–285. https://doi.org/10.1152/jn.1961.24.3.272

Stuart, G., N. Spruston, and M. Häusser. 2007. Dendrites. Oxford University Press, Oxford; New York. 560 pp.

Tada, A., I. Suzuki, S. Im, M.B. Davis, J. Cornelius, G. Babcock, J.J. Nordlund, and Z.A. Abdel-Malek. 1998. Endothelin-1 is a paracrine growth factor that modulates melanogenesis of human melanocytes and participates in their responses to ultraviolet radiation. *Cell Growth Differ.* 9: 575–584.

Takacs, C.N., U. Andreo, R.L. Belote, J. Pulupa, M.A. Scull, C.E. Gleason, C.M. Rice, and S.M. Simon. 2017a. Green fluorescent protein-tagged apolipoprotein E: A useful marker for the study of hepatic lipoprotein egress. *Traffic.* 18:192–204. https://doi.org/10.1111/tra.12467

Takacs, C.N., U. Andreo, V.L. Dao Thi, X. Wu, C.E. Gleason, M.S. Itano, G.S. Spitz-Becker, R.L. Belote, B.R. Hedin, M.A. Scull, et al. 2017b. Differential Regulation of Lipoprotein and Hepatitis C Virus Secretion by Rab1b. *Cell Reports.* 21:431–441. https://doi.org/10.1016/j.celrep.2017.09.053

Tinkle, C.L., T. Lechler, H.A. Pasolli, and E. Fuchs. 2004. Conditional targeting of E-cadherin in skin: insights into hyperproliferative and degenerative responses. *Proc. Natl. Acad. Sci. USA.* 101:552–557. https://doi.org/10.1073/pnas.0307437100

Valyi-Nagy, I.T., G. Hirka, P.J. Jensen, I.M. Shih, I. Juhasz, and M. Herlyn. 1993. Undifferentiated keratinocytes control growth, morphology, and antigen expression of normal melanocytes through cell-cell contact. *Lab. Invest.* 69:152–159.

Wu, X., and J.A. Hammer. 2014. Melanosome transfer: it is best to give and receive. *Curr. Opin. Cell Biol.* 29:1–7. https://doi.org/10.1016/j.ceb.2014.02.003

Yohn, J.J., J.G. Morelli, S.J. Walchak, K.B. Rundell, D.A. Norris, and M.R. Zamora. 1993. Cultured human keratinocytes synthesize and secrete endothelin-1. *J. Invest. Dermatol.* 100:23–26. https://doi.org/10.1111/1523-1747.ep12349932

Yuste, R., and W. Denk. 1995. Dendritic spines as basic functional units of neuronal integration. *Nature.* 375:682–684. https://doi.org/10.1038/375682a0

JCB

Supplemental material

Belote and Simon, https://doi.org/10.1083/jcb.201902014

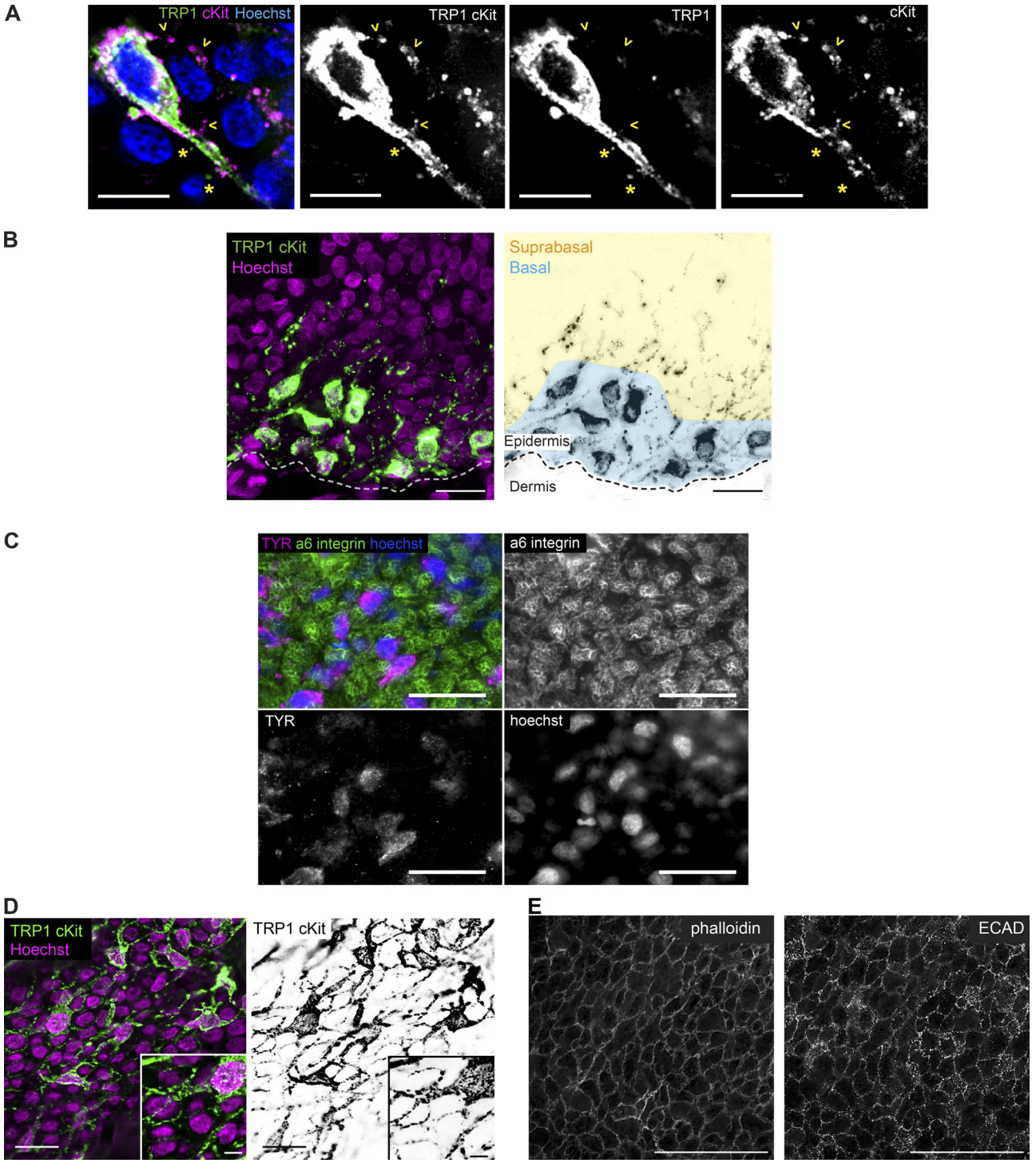

Figure S1. **Melanocyte morphology within neonatal foreskin. (A)** Melanocyte-specific antibody cocktail (α-TRP1 and α-c-Kit) provides extensive labeling of melanocytes in human epidermis. Yellow asterisk indicates region only recognized by α-TRP1; yellow arrowhead indicates regions only recognized by α-c-Kit. Scale bars, 10 µm. **(B)** Angled cross-section of intact neonatal foreskin. Dotted line demarcates the basement membrane. Blue region highlights melanocyte cell bodies in the basal layer. Orange indicates suprabasal layers. Scale bars, 20 µm. **(C)** The epidermis retains the basal layer of cells including keratinocytes (green, α6-integrin–positive cells) and melanocytes (magenta, tyrosinase [TYR]-positive cells) upon removal from the dermis via dispase. Scale bars, 25 µm. **(D)** Melanocytes (green: melanocyte-specific antibody cocktail, TRP1 and cKIT combined) have extensive dendritic branching across the epidermal basal-proximal layer of human neonatal foreskin. Scale bars, 20 µm. **(E)** Cytoskeleton morphology, assessed by phalloidin binding of F-actin, and cell–cell adhesion assessed by ECAD expression across the basal layer of an epidermal sheet from neonatal foreskin. Scale bars, 100 µm.

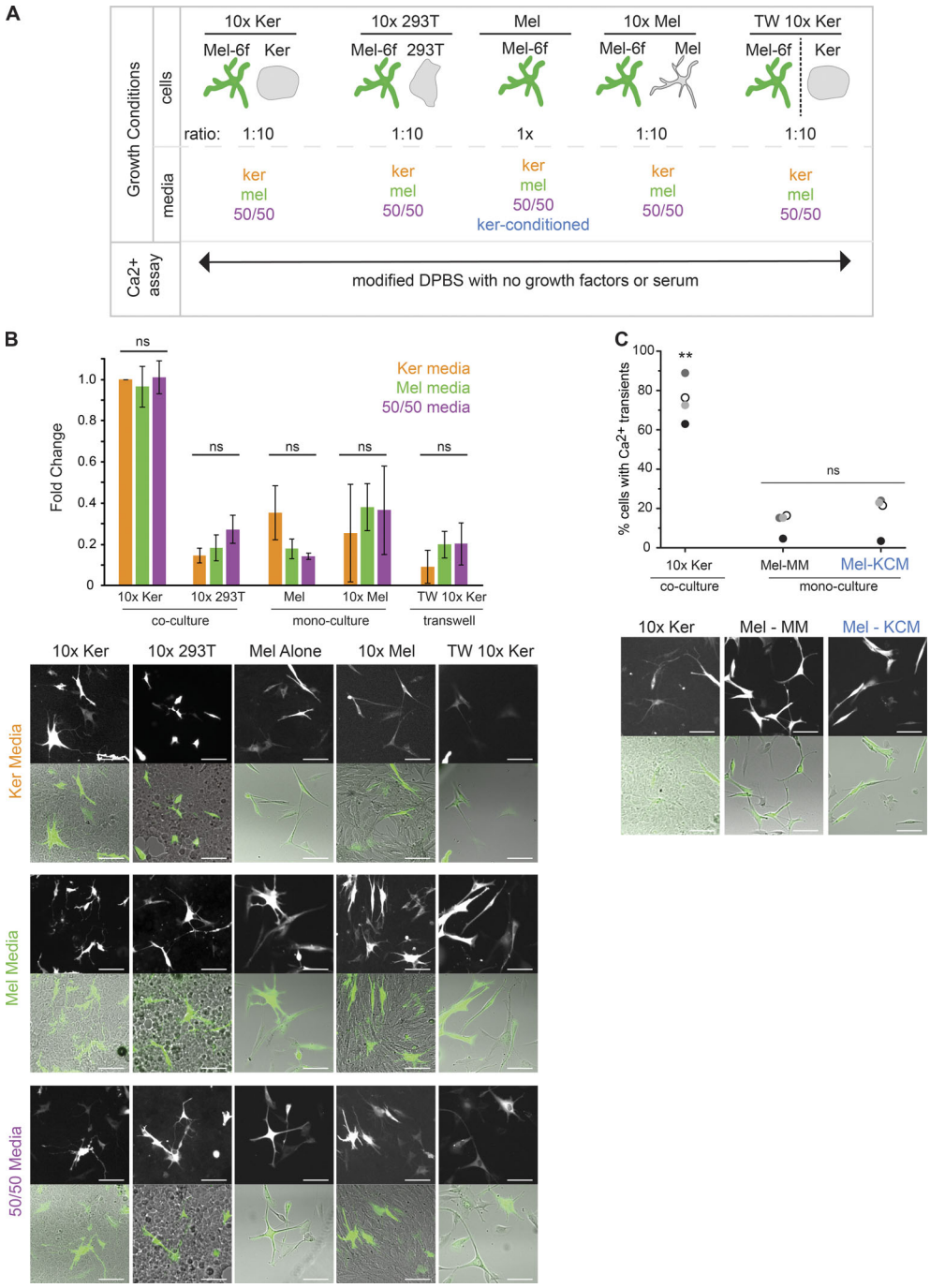

Figure S2. **Number of melanocytes with Ca^{2+} transients is keratinocyte dependent and not dependent on growth conditions. (A)** Experimental design for determining the effect of growth conditions on melanocyte Ca^{2+} transients: GCaMP6f-expressing melanocytes were cultured with either keratinocytes (10× Ker), 293Ts (10× 293T), melanocytes not expressing GCAMP6f (10× Mel), or alone (Mel). Each culture type was grown in either standard co-culture media (ker, orange), melanocyte media (mel, green), 1:1 mix of melanocyte/keratinocyte media (50/50, purple), or keratinocyte conditioned media (ker conditioned or KCM, blue). For all conditions, the final growth media contained 1.06 mM $CaCl_2$. All cultures were then washed and imaged in modified DPBS, with 1.06 mM $CaCl_2$ to determine the number of GCaMP6f-expressing melanocytes with Ca^{2+} transients in the absence of exogenous growth factors. **(B)** Fold change in the percent of GCaMP6f-expressing melanocytes with Ca^{2+} transients in the indicated conditions: keratinocyte growth media (orange), melanocyte growth media (green), 50/50 media (purple). Fold change: the ratio of the given culture condition to the corresponding biological replicate's 10× Ker in keratinocyte growth media. One-way ANOVA analysis within each culture type showed no difference between growth media; ns, not significant. Data represented as mean ± SD; $n \geq 3$ biological replicates per culture and media condition. Representative images of GCaMP6f-expressing melanocytes in co-culture or mono-culture grown in the indicated conditions. **(C)** Percentage of GCaMP6f-expressing melanocytes with at least one Ca^{2+} transient grown in the indicated conditions. One-way ANOVA $F(2,9) = 59.68$, $P = 0.05$. $n = 4$ co-cultures from different skin donors; **, $P < 0.00005$; ns, not significant: $P > 0.05$. Representative images of GCaMP6f-expressing melanocytes in co-culture or mono-culture grown in the indicated conditions: 10× Ker, normal co-culture conditions with 10× keratinocytes in normal co-culture growth media; Mel-MM, melanocytes in mono-culture grown in melanocyte growth media; Mel-KCM, melanocytes in mono-culture grown in keratinocyte conditioned co-culture media. All scale bars, 200 µm.

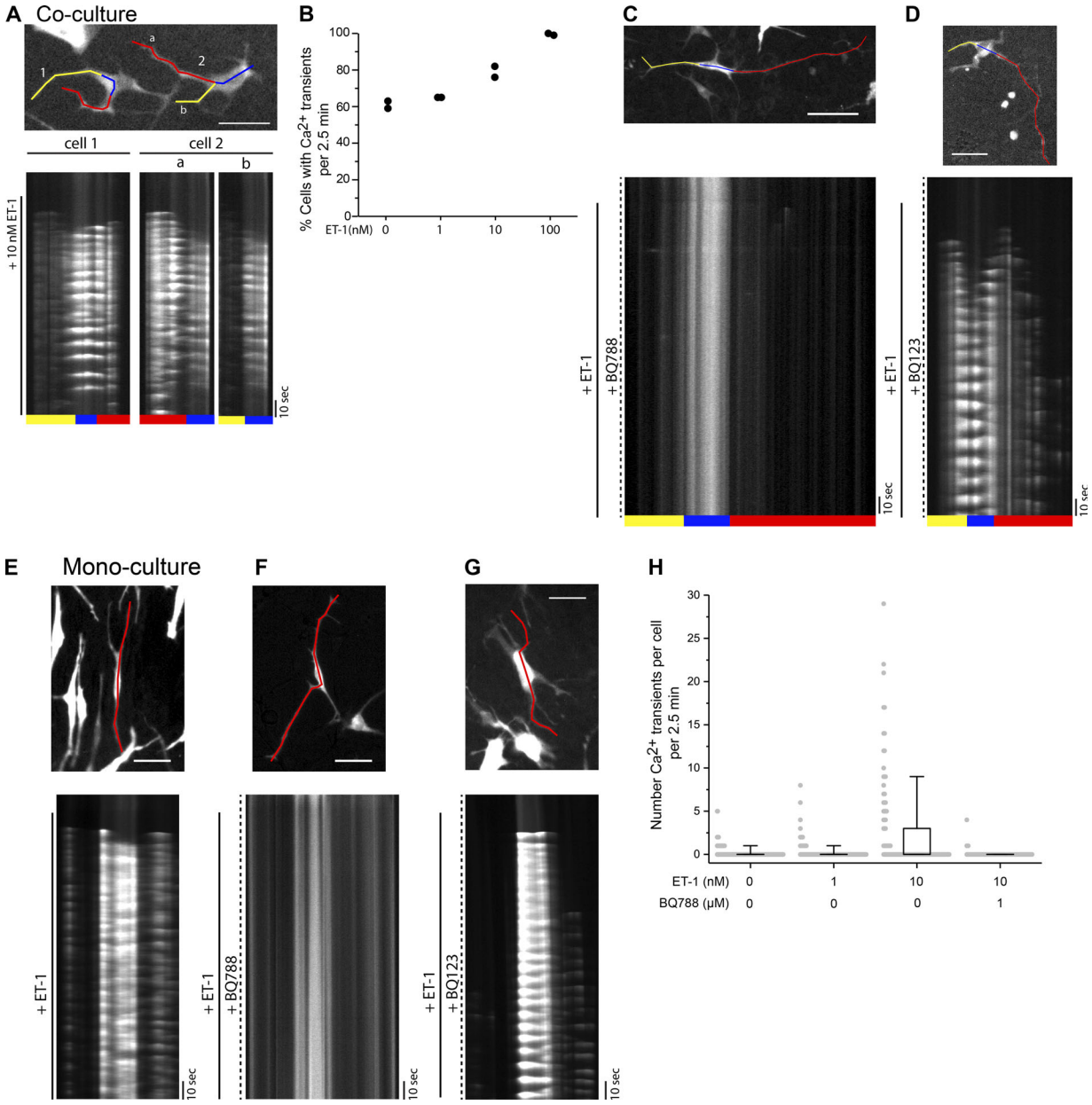

Figure S3. **ET_B-mediated dose dependent response to ET-1 in mono- and co-cultured melanocytes. (A–D)** ET-1 stimulation of co-cultured melanocytes. **(A)** 10nM ET-1 induces Ca^{2+} transients across the entire melanocyte. Top: Two representative melanocytes (cell 2 is the same cell from Fig. 4 C). Scale bar, 100 µm. Bottom: Kymographs from corresponding color coded lines in top panel; black line denotes change to imaging media containing 10 nM ET-1. **(B)** Percent of melanocytes with Ca^{2+} transients in the presence of 0, 1, 10, or 100 nM ET-1 during a 2.5-min imaging period. *n* = 2 co-cultures from two different donor skin cells. **(C)** ET_B antagonist BQ788 abrogates ET-1 induced Ca^{2+} response in co-cultured melanocytes. Top: Representative melanocyte. Scale bar, 150 µm. Bottom: Kymograph from corresponding color-coded line in top panel; solid black line denotes change to imaging media containing 10 nM ET-1 while maintaining 1 µM BQ788 (dashed black line). **(D)** BQ123 inhibition of ET_A did not inhibit melanocyte Ca^{2+} response to 10nM ET-1. Top: Representative melanocyte. Scale bar, 100 µm. Bottom: Kymograph from corresponding color coded line in top panel; solid black line denotes change to imaging media containing 10nM ET-1 while maintaining 1 µM BQ123 (dashed black line). **(E–H)** ET-1 stimulation of mono-cultured melanocytes. **(E)** 10 nM ET-1 induces Ca^{2+} oscillations across the entire melanocyte. Top: Representative melanocyte. Bottom panel: Kymographs from corresponding line in top panel; black line denotes change to imaging media containing 10 nM ET-1. **(F)** ET_B antagonist BQ788 abrogates ET-1 induced Ca^{2+} response in mono-cultured melanocytes. Top: Representative melanocyte. Bottom: Kymograph from line in top panel; solid black line denotes change to imaging media containing 10 nM ET-1 while maintaining 1 µM BQ788 (dashed black line). **(G)** BQ123 inhibition of ET_A did not inhibit melanocyte Ca^{2+} response to 10 nM ET-1. Top: Representative melanocyte. Bottom: Kymograph from corresponding line in top panel; solid black line denotes change to imaging media containing 10 nM ET-1 while maintaining 1 µM BQ123 (dashed black line). **(H)** Number of Ca^{2+} transients per mono-cultured melanocyte during 2.5 min in the presence of 0 nM ET-1, 1 nM ET-1, 10 nM ET-1, or 10 nM BQ788 (*n* = 159, 107, 107, and 52 cells from 2, 1, 1, and 1 cultures, respectively). All scale bars, 100 µm.

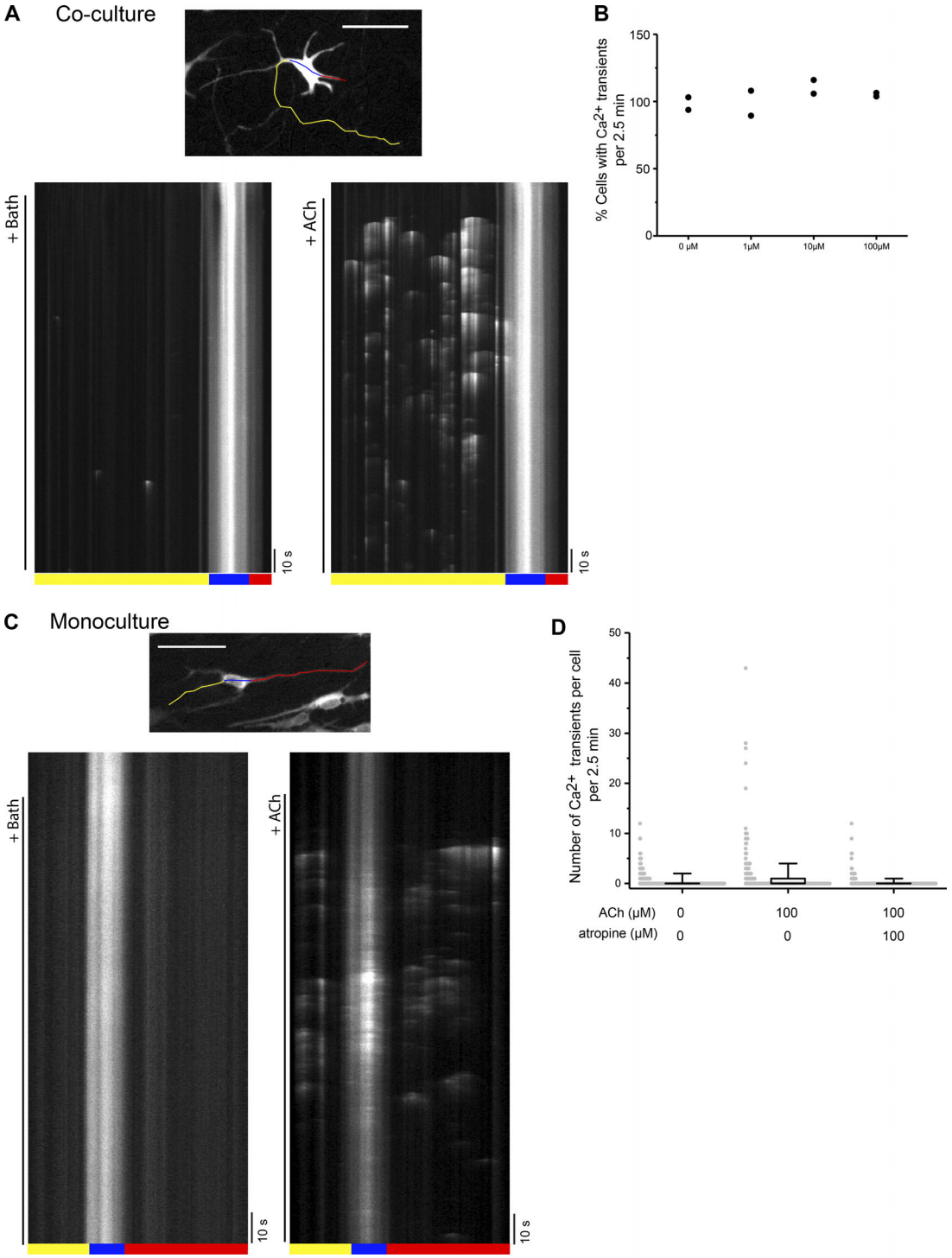

Figure S4. **Melanocyte response to ACh in mono- and co-culture. (A)** Representative melanocyte, in co-culture with keratinocytes, with Ca^{2+} response to 100 µM ACh. Bottom: Kymograph from corresponding color coded line in top panel; black line denotes change to fresh imaging media (left, "bath") or change to imaging media containing 100 µM ACh (right, +ACh). **(B)** ACh does not increase the number of melanocytes with Ca^{2+} transients during 2.5 min. *n* = 2 co-cultures from different donor skin cells per condition. **(C)** Representative melanocyte, from mono-culture, with Ca^{2+} response to 100 µM ACh. Bottom: Kymograph from corresponding color coded line in top panel; black line denotes change to fresh imaging media (left, Bath) or change to imaging media containing 100 µM ACh (right, +ACh). Scales bar, 150 µm. **(D)** Number of Ca^{2+} transients per mono-cultured melanocyte during 2.5 min in the presence of 0 µM ET-1, 100 µM ET-1, or 100 µM atropine (*n* = 405, 203, and 202 cells from 4, 2, and 2 cultures from different donor skin cells, respectively). All scale bars, 150 µm.

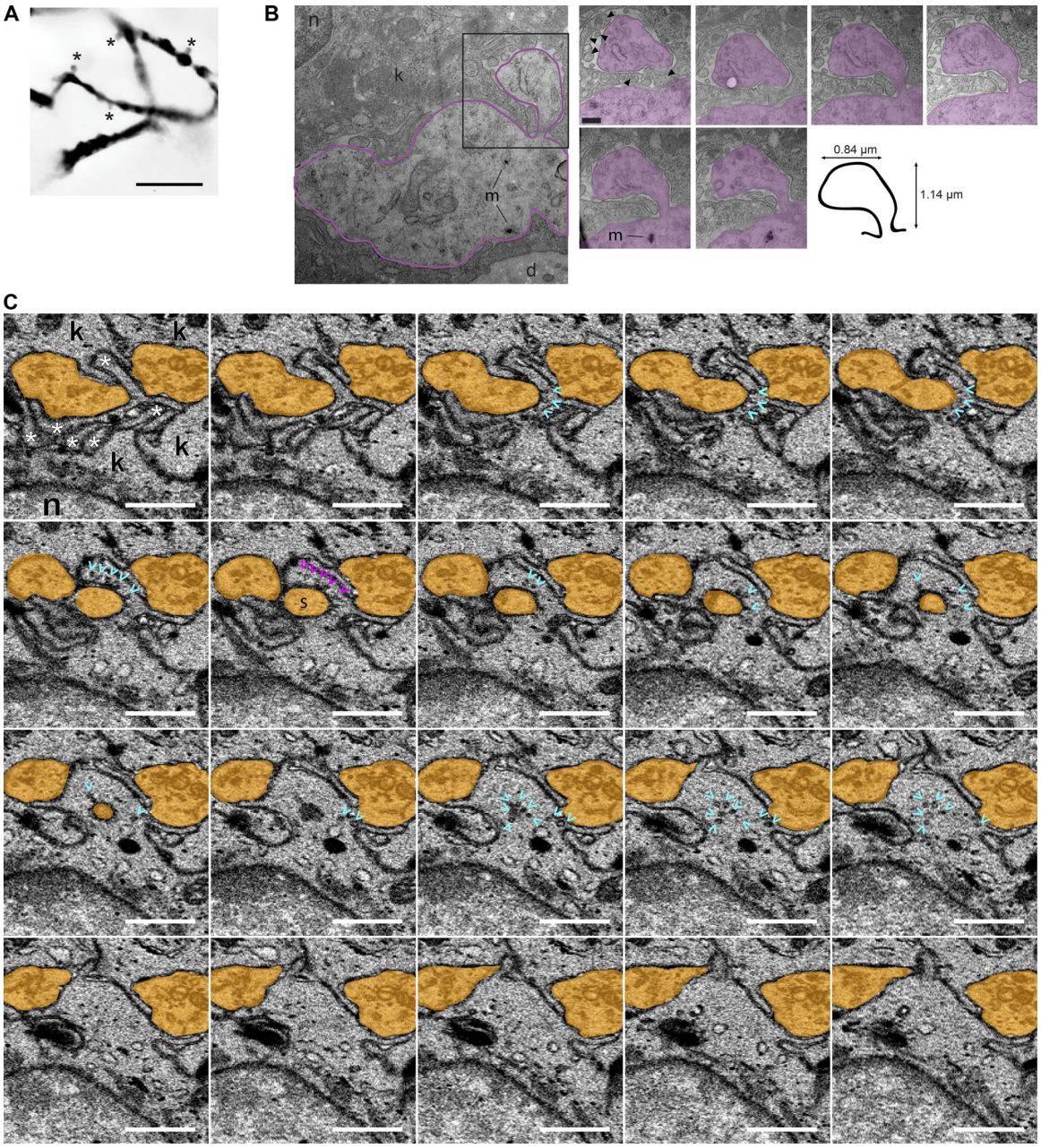

Figure S5. **Ultrastructure of melanocyte dendritic spine-like structures and pooled vesicles in adjacent keratinocyte. (A)** Small protrusions (*) on melanocyte dendrite from Lucifer yellow microinjected melanocyte in Fig. 1 B. Scale bar, 10 µm. **(B)** TEM serial sections (50–100 nm) of a representative spine-like structure from intact neonatal foreskin with illustration depicting the morphology and size of the spine-like structure. Melanocyte dendrite in purple; n, nucleus; d, dermis; arrowhead, keratinocyte processes. Note the melanosomes and electron-lucent cytoplasm differentiate the melanocyte from the surrounding keratinocytes. Scale bar, 250 nm. **(C)** Serial 30-nm z sections from FIB-SEM data that were used to generate the 3D reconstruction in Fig. 10 E. Magenta arrowheads correspond to vesicles in Fig. 10 E; "s" corresponds to region of melanocyte (orange) that is adjacent to keratinocyte vesicles; *, keratinocyte projections; k, keratinocyte; cyan arrowhead, vesicles. Scale bar, 1 µm.

Table S1. **Quantification of melanocyte dendrites and spines from FIB-SEM reconstruction**

Melanocyte	Dendrites total[a] (complete[b])	Branches with spines	Spines d(CB)[c]	Spine density per branch[d]
Mel 1	6 (3)	4	10 (1)	3, 2, 1, 1
Mel 2 (Fig. 10 D and Fig. S5 C)	9 (8)	5	7 (0)	3, 1, 1, 1, 1
Mel 3 (Fig. 2, F–H)	7 (4)	4	12 (0)	6, 2, 3, 1
Mel 4	5 (2)	1	1 (0)	1

The number of dendrites and spines from the four melanocytes reconstructed using FIB-SEM within a 30 × 27 × 27-µm volume of neonatal foreskin at 30-nm z resolution and an XY pixel size of 14–18 nm.
[a]Number of dendrites present, including primary and secondary branches and those that were continued beyond the volume of tissue that was imaged.
[b]Number of dendrites that were fully reconstructed within the imaged volume of tissue.
[c]d, Number of spines on a dendrite; CB, number of spines on the body. All melanocytes had some cell body present in the imaged volume, and all cell bodies continued outside of the imaged volume; thus, no cell body was fully reconstructed.
[d]Number of spines per 10 µm on each branch from footnote a.

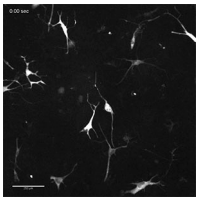

Video 1. **Ca^{2+} Transients in melanocytes co-cultured with keratinocytes.** Related to Fig. 3. Time-lapse epifluorescence microscopy of the fluorescence signal from a GCaMP6f calcium reporter expressed in melanocytes that were co-cultured with keratinocytes. The cells were incubated in the absence of external serum or growth factors. Acquisition rate: streaming 250 ms. Display rate: 40 frames/s.

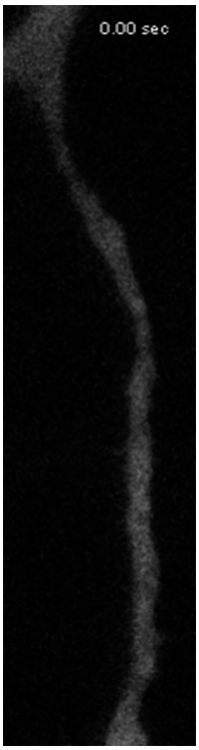

Video 2. **Co-cultured melanocyte dendritic Ca^{2+} transients.** Related to Fig. 4, B and C. Time-lapse epifluorescence microscopy of the fluorescence signal from GCaMP6f in a single dendrite in Fig. 4, B and C, from a melanocyte that was co-cultured with keratinocytes in the absence of external serum or growth factors. Acquisition rate: streaming 250 ms. Display rate: 40 frames/s.

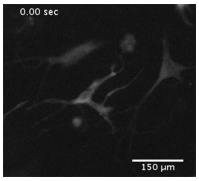

Video 3. **Melanocyte response to 10 nM ET-1 in co-culture with keratinocytes.** Related to Fig. 6. Time-lapse epifluorescence microscopy of the fluorescent signal from the calcium reporter GCaMP6f expressed in melanocytes that were co-cultured with keratinocytes. The fluorescence is shown before and after the addition of 10 nM ET-1 (appearance of "+10nM ET-1" in bottom left corner of video). Acquisition rate: streaming 250 ms. Display rate: 40 frames/s.

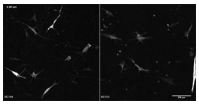

Video 4. **BQ788 but not BQ123 inhibits co-cultured melanocyte Ca^{2+} response to ET-1.** Related to Fig. 6, A–C; Fig. 7 A; and Fig. S3, C and D. Time-lapse epifluorescence microscopy of the fluorescent signal from the calcium reporter GCaMP6f expressed in melanocytes that were co-cultured with keratinocytes. Fluorescence is shown before and after the addition of 10 nM ET-1 (appearance of "+10nM ET-1" in bottom left corner of the panel) in the presence of BQ788 (left panel) or BQ123 (right panel). Acquisition rate: streaming 250 ms. Display rate: 40 frames/s.

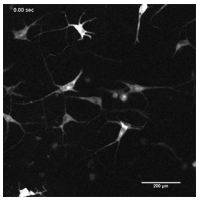

Video 5. **Co-cultured melanocyte response to 100 µM Ach.** Related to Fig. 6 (F and G) and Fig. S4 A. Time-lapse epifluorescence microscopy of the fluorescence signal from the calcium reporter GCaMP6f expressed in melanocytes that were cultured with keratinocytes. The fluorescence is shown before and after the addition of 100 µM ACh (appearance of "+100 µM ACh" at bottom video). Acquisition rate: streaming 250 ms. Display rate: 40 frames/s.

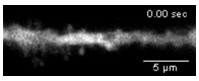

Video 6. **Ca^{2+} transients in co-cultured melanocyte dendrite and dendritic spine.** Related to Fig. 9. Time-lapse epifluorescence microscopy of the fluorescence from the calcium reporter GCamP6f in a single dendrite from a melanocyte that was cultured with keratinocytes. Acquisition rate: streaming 250 ms. Display rate: 40 frames/s.

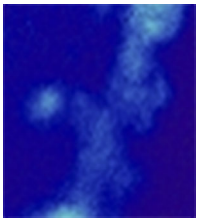

Video 7. **Ca^{2+} transient in co-cultured melanocyte dendritic spines.** Related to Fig. 9. Time-lapse epifluorescence microscopy of the fluorescence from the calcium reporter GCamP6f in a single dendrite, with dendritic spine-like structures on a melanocyte that was cultured with keratinocytes. Video corresponds to regions 1, 2, and 3 in Fig. 3 B. Blue indicates low GCaMP6f signal and red indicates high GCaMP6f signal. Acquisition rate: streaming 250 ms. Display rate: 40 frames/s.